Long-term support of an active subglacial hydrologic system in Southeast Greenland by firn aquifers

Kristin Poinar[1], Christine F. Dow[2], Lauren C. Andrews[3]
[1]University at Buffalo, [2]University of Waterloo, [3]NASA Goddard Space Flight Center

Corresponding authors: K. Poinar (kpoinar@buffalo.edu), C. F. Dow (christine.dow@uwaterloo.ca), L. C. Andrews (lauren.c.andrews@nasa.gov)

Key Points

- High-elevation firn-aquifer water drainage drives evolution of the subglacial hydrologic system >30 km inland, potentially affecting outlet-glacier speed
- Persistent input of water from firn aquifers can maintain subglacial channels outside the melt season and across years
- The timing and duration of firn-aquifer water delivery to the bed is an important but under-constrained variable in ice sheet hydrology

Abstract

The state of the subglacial hydrologic system, which can modify ice motion, is sensitive to the volume and rate of meltwater reaching it. Bare-ice regions rapidly transport meltwater to the bed via moulins, while in certain accumulation-zone regions, meltwater first flows through firn aquifers, which can introduce a substantial delay. We use a subglacial hydrological model forced with idealized meltwater input scenarios to test the effect of this delay on subglacial hydrology. We find that addition of firn-aquifer water to the subglacial system elevates the inland subglacial water pressure while reducing water pressure and enhancing subglacial channelization near the terminus. This effect dampens seasonal variations in subglacial water pressure and may explain regionally anomalous ice-velocity patterns observed in Southeast Greenland. As surface melt rates increase and firn aquifers expand inland, it is crucial to understand how inland drainage of meltwater affects the evolution of the subglacial hydrologic system.

Plain language summary

The flow of ice and meltwater from the Greenland Ice Sheet into the ocean affects sea levels. Ice flow is sensitive to meltwater that travels underneath the glacier. Where and when that water reaches the glacier bed shapes the water channel network under the glacier. We use a computer model to analyze how firn aquifers, newly discovered meltwater pockets that sit dozens of meters below the ice-sheet surface in East Greenland, change the water channel network under local glaciers. We find that the firn-aquifer water supply can maintain a water channel network under the glacier that changes less over each season, compared to areas without firn-aquifer water. This subglacial channelization could explain observations of steadier glacier flow in locations with firn aquifers.

1. Introduction

Delivery of surface meltwater to the base of an ice sheet can alter the subglacial hydrologic system and affect seaward ice flow (e.g., Bartholomew et al., 2010; Sundal et al., 2011; Hoffman et al., 2011). Determining what controls the development of the subglacial drainage network is important for understanding ice-sheet mass balance (Parizek & Alley, 2004; Shannon et al., 2013). Given newly observed mechanisms modifying surface meltwater storage (Forster et al., 2014; Machguth et al., 2016) and anticipated near-future increases in Greenland meltwater production (e.g., Fettweis et al., 2013; Mottram et al., 2017), characterizing the relationship between surface meltwater and subglacial hydrologic system development is crucial for projecting the evolution of ice-sheet mass imbalance.

The time lag between formation of surface meltwater and its descent to the bed of the Greenland Ice Sheet is spatially variable. In the bare-ice zone, supraglacial streams and lakes

conduct meltwater into moulins and crevasses quickly, within the period of one melt season (Das et al., 2008; Smith et al., 2015). This drives a seasonal evolution of the subglacial hydrologic system from inefficient to efficient drainage states, first increasing and then reducing basal sliding and ice motion (Bartholomew et al., 2011a; Chandler et al., 2013; Hoffman et al., 2011). Bare-ice zones are more extensive in western Greenland due to more gradual surface slopes.

In eastern Greenland, where annual snowfall is substantial, firn aquifers collect meltwater and retain it for multiple years, delaying input of seasonal water to the subglacial system (Forster et al., 2014; Kuipers Munneke et al., 2014). Water discharge from firn aquifers can drive crevasses to the bed, providing a direct path for firn-aquifer water to the subglacial environment (Poinar et al., 2017). The effect of firn-aquifer drainage on the subglacial hydrologic system is presently unknown.

Firn aquifers currently occupy areas low in the accumulation zone around much of the Greenland Ice Sheet (Miège et al., 2016), with inland expansion anticipated in future warm climates (Steger et al., 2017a). If new surface-to-bed connections are made at inland locations, the subsequent evolution of the subglacial hydrologic system may alter ice dynamics (e.g., Bartholomew et al., 2011b; Clason et al., 2015; Doyle et al., 2014; Poinar et al., 2015; Christoffersen et al., 2018). Here, we implement a modeling study whereby a series of idealized scenarios drain surface water to the bed at low-elevation locations and at higher elevations through the downstream end of a firn aquifer. We test the sensitivity of the subglacial hydrologic system to these melt input scenarios to provide the first constraints on the effects of firn-aquifer drainage on the Greenland subglacial hydrologic system.

2. Methods

2.1 Idealized model domain

Helheim Glacier (Figure 1a) is a large tidewater glacier in Southeast Greenland with an active subglacial hydrologic system (Andersen et al., 2011; Bevan et al., 2015; Everett et al., 2016). Surface melt and fjord conditions may drive local dynamic thinning (Bevan et al., 2015; Everett et al., 2016; Kehrl et al., 2017; Straneo et al., 2011). Firn-aquifer water has been detected by radar at surface elevations above ~1500 m and likely locally drains through crevasses to the bed (Miège et al., 2016; Poinar et al., 2017). Using these basic characteristics, we constructed a model domain with an idealized, 680-m deep trough spanning the lowermost 30 km and an overdeepening within 8 km of the terminus (ST.2; Howat et al., 2014, 2015; Morlighem et al., 2014, 2017a, 2017b). We supply basal melt uniformly across the catchment (ST.4; Aschwanden et al., 2012; MacGregor et al., 2016). We apply the Glacier Drainage System (GlaDs) model (Werder et al., 2013) to investigate the evolution of the subglacial hydrologic system beneath an

idealized outlet glacier downstream of a draining firn aquifer (Figure 1b) (ST.3; de Fleurian et al, 2018; Dow et al., 2016, 2018; Wei et al, 2018).

2.2 Water inputs to the subglacial system

We developed model experiments that test the effects of five different meltwater-input scenarios on subglacial hydrologic system development over seasonal and multi-year timescales. The control experiment includes only low-elevation water inputs; the remaining four experiments also include firn-aquifer water inputs supplied over a horizontal distance of 10 km. We designed these experiments to simulate water discharge to the subglacial system by hydrofracture of a crevasse to the base of the ice sheet, which delivers an immediate water flux, followed by continued drainage of firn-aquifer water at similar or slower rates (ST.4.3; Poinar et al., 2017;). The firn aquifer experiments all receive the same meltwater input volume to the subglacial system, which is ~10% greater than in the low-elevation experiment (Figure 1c, 2e).

2.2.1 Low-elevation meltwater supply

In the terminus region of outlet glaciers, water flows through individual moulins and crevasses to the ice-sheet bed (Everett et al., 2016; Lampkin & VanderBerg, 2013). In the lowest 20 km of our model domain (surface elevation *s* ~100–900 m), we supplied meltwater to the bed over each melt season at 30 quasi-random sites (Figure 1d), a majority of which (25) overlie the basal trough. We divided a total meltwater flux of 4.9×10^{8} $m^{3}\cdot yr^{-1}$, derived from the MERRA-2 climate reanalysis dataset (Gelaro et al., 2017), evenly among 30 sites, and input this water seasonally according to the 1981–2016 climatological average. The 3-day time step of our model output excludes effects of the diurnal melt cycle and ~1-day surface routing process (Andersen et al., 2011), timescales which have limited effect on the total downglacier ice displacement (Hewitt, 2013). Details are available in ST.4.2 (Banwell et al., 2013; Doyle et al., 2013; McGrath et al., 2011; Meierbachtol et al., 2013; Phillips et al, 2011).

2.2.2 Mid-elevation absence of meltwater supply

The accumulation zone and perennial snow cover begins immediately above the main trunk of Helheim Glacier (Noël et al., 2016). In accumulation areas with moderate snowfall (<~2 $m\cdot y^{-1}$), nearly all meltwater refreezes within the snow and firn (Kuipers Munneke et al., 2014). These conditions represent *s* ~900–1500 m (~20–40 km from the terminus) in the Helheim region; thus, we prescribe zero meltwater input to the basal system in this region of our domain (Figure 1d).

2.2.3 High-elevation firn-aquifer meltwater supply

The firn aquifer may supply water to the bed continuously or episodically (Poinar et al., 2017, Legchenko et al., 2018), and, because meltwater takes years to decades to travel through the

firn-aquifer system (Miller et al., 2017), the time of year that water reaches the bed is not known. To account for temporal uncertainty in firn aquifer discharge patterns, we developed four firn-aquifer drainage hydrographs. First, we use a step function, with firn-aquifer input initiating on August 1 of Year 1 and continuing steadily for 4 years. Next, we test two ramp scenarios, with input initiating on August 1 of Year 1: a “long ramp”, in which discharge steadily declines over the remainder of the four-year model run, and a series of “short ramps” of seven-month discharge periods separated by month-long pauses. Finally, we test a “seasonal ramp” scenario, in which aquifer water discharges only within the melt season, declining from a June 1 maximum to zero by September 15. We designed these scenarios to represent different hydraulic conductivities within the firn aquifer and different degrees to which crevasses may maintain connections to the bed over time. Based on previous work (Miège et al., 2016, Poinar et al, 2017), we represent the input of firn-aquifer water to the subglacial system as a 10-km-long line source at ~1500 m elevation, 40 km from the terminus (Figure 1d), at an average rate of 50×10^6 $m^3 \cdot y^{-1}$. In each scenario, the total volume of firn-aquifer water supplied to the system is only 10% of that supplied through the low-elevation inputs.

Regional firn-aquifer observations are currently made approximately yearly, so sub-annual drainage events such as our short-ramp or seasonal-ramp scenarios may be undetected. Formation and advection of crevasses may allow either shorter or longer connections than we model here (Poinar et al., 2017). Overall, the full plausibility of our firn-aquifer drainage scenarios is underconstrained.

3. Results

Each GlaDS model simulation consisted of a spin-up to steady state without surface water input, one year with only low-elevation water inputs (not shown in figures), and a four-year simulation period with one of the five meltwater input scenarios described above. We evaluate the results of each model run by examining the distributed water layer thickness, subglacial channel extent and persistence (Figure 2; Video S1), mean and time-varying water pressures, and residence time of water within the subglacial system (Figure 3; Video S2). To constrain possible differences between regions with and without firn aquifer drainage, we use the low-elevation-only scenario as a control against which to compare the results of the four firn-aquifer water input scenarios.

3.1 Subglacial channel size and persistence

In all scenarios, we observed a dense row of subglacial channels in the overdeepening in the bottom 4 km of our domain (Figure 2a–e). We focus our analysis away from these features because they likely originate from the oceanic boundary condition (Fried et al., 2015).

In the low-elevation scenario, two to three primary channels formed in the lower 10 km of the glacier each melt season (Figure 2a). These channels had cross-sectional area (*c.s.a.*) > 12 m^2 and were fed by smaller channels (*c.s.a.* < 3 m^2) that collapsed by the end of the melt season (Video S1). The summertime subglacial water sheet thickness decreased each year as the largest channels grew (Figure 2f). Because hydrologic models with land-terminating boundary conditions do not capture this behavior, we hypothesize that the oceanic boundary allowed small channels (*c.s.a.* < 0.5 m^2) to persist through the winter (Fried et al., 2015; Schild et al., 2016).

In all firn-aquifer drainage scenarios, the sudden input of high-elevation meltwater during the first melt season rapidly increased subglacial water volume without immediately driving channel development. The subglacial system in the upper model domain remained inefficient until late winter, when the firn-aquifer water reached the steeper hydraulic gradient 30 km from the terminus. There, small *(c.s.a.* < 2 m), isolated channels formed, then expanded both upstream and downstream (Video S1). During the second melt season, larger channels *(c.s.a.* > 2 m) reached inland more quickly than in the low-elevation case, and persisted for months following the melt season (Figure 2b–e; Video S1). Two to three primary channels formed >20 km above the trough during the second melt season and persisted for multiple years (Figures 2b–e; S3–S6). These channels joined within the upper 5 km of the trough into one primary channel under ~10 km of the outlet glacier. During the third melt season, smaller, ~45°-inclined channels connected water input sites to this channel. The persistence of the primary channel, the oceanic boundary condition, and the smooth topographic gradient within the trough likely drove this lateral water flow.

The episodic nature of the short-ramp firn-aquifer water inputs induced a greater variation in channel size and extent than seen in the step or long-ramp scenarios (Figure 2d; Video S1). When firn-aquifer input coincided with the melt season (Years 2 and 4), we observed more upglacier channels than when the water inputs were temporally offset (Years 1 and 3). These channels carried firn-aquifer water to the same primary channel in the outlet glacier each year (Figure 3d; Video S1). The short-ramp scenario generated both the highest-elevation channels (*c.s.a*. > 0.5 m^2 nearly to the aquifer site at s = 1500 m) and the most persistent channels (Figure 2g).

Seasonal firn-aquifer inputs (Figure 2e) drove development of a downglacier channel network that was more similar to the low-elevation control case than the other firn-aquifer runs. Compared to other firn-aquifer runs, the seasonal firn-aquifer run created a less-developed central downglacier channel that was linked to input sites by fewer high-angle channels. The distributed system sheet thickness in the upper ablation zone (~20 km from the terminus) remained higher late in each melt season compared to other firn-aquifer runs, yet was still lower than in the low-elevation control case. Two upglacier channels (>20 km from terminus) persisted after the first melt season, allowing more rapid evacuation of the aquifer water during the second melt season (Figure 2e; Video S1). By the beginning of Year 3, the subglacial system in

the seasonal-aquifer run resembled that of the low-elevation run, with low water volumes and a minimal channel network. During the third melt season, the water volume remained high as the downglacier channel network reformed at a comparable rate to the low-elevation run, which again allowed efficient removal of seasonal melt water in Year 4. Our particular subglacial system shows ~2-year periodicity when forced with seasonal firn-aquifer input.

Overall, firn-aquifer water inputs induced larger, more spatially extensive subglacial channels that persisted into or through winter. Water inputs outside the melt season maintained the channel network both up- and downglacier, but even firn-aquifer input during the melt season only allowed persistence of a wintertime network, in some years. When the channel network persisted, it greatly dampened melt-season variations in the distributed system water sheet thickness (Figure 2g).

3.2 Evolution of subglacial water pressure

In the low-elevation scenario, the domain-averaged subglacial water pressure peaked ~60 days into the melt season, then gradually declined to winter values (Figures 3a; 3e; S1–S2). In scenarios with firn-aquifer water input, the initiation of firn-aquifer drainage during the first melt season abruptly increased the upstream water pressure (Figures 3b–e; S1–S5).

In the firn-aquifer step and long-ramp scenarios, the firn-aquifer water traveled downglacier at ~40 $m \cdot d^{-1}$ ($5 \times 10\text{-}4$ $m \cdot s\text{-}1$) over the autumn and winter, while water pressures remained locally high (Video S1). In winter of Year 2, the water reached the more steeply sloped trough and accelerated downglacier at ~1000 $m \cdot d^{-1}$ (0.01 $m \cdot s\text{-}1$) without forming sizable channels. During the second melt season, the steep hydraulic gradient created by the high-elevation firn-aquifer-sourced water drove earlier formation of ablation-zone channels (<20 km) and inland channels (>30 km), compared to the first year and the low-elevation run. The inland channels persisted over remaining winters and reduced the melt-season water pressures near low-elevation water input sites by >30%, compared to the low-elevation control case (Figure 3a–c). Overall, the firn-aquifer input raised mean water pressures at high elevations but reduced mean water pressures at lower elevations (Figures 3b–c; S7).

In the firn-aquifer short-ramp scenario, the Year 1 firn-aquifer input raised the domain-averaged water pressure, which persisted over winter until substantial subglacial channels formed in Year 2 (Figures 3d; S1; Video S1). Each water input event increased the domain-averaged water pressure, followed by a decline. The variability of the short-ramp inputs created the highest inland water pressures and drove formation of the most centralized inland channel network (Figures 3d; S5; S7).

In the seasonal ramp firn-aquifer scenario, the firn-aquifer water traveled downglacier at ~70 $m \cdot d^{-1}$ ($8 \times 10\text{-}4$ $m \cdot s\text{-}1$) over the melt season and reached the trough during the first winter. Thus, the firn-aquifer water had minimal effect on the downglacier system in Year 1. However, this

low-elevation, wintertime subglacial water conditioned the system to quickly form sizable channels at the beginning of the second melt season (Video S2), which reduced the domain-averaged water pressure throughout Year 2. By the end of Year 2, the subglacial system closely resembled its initial state, and in Year 3 its evolution was much the same as in Year 1.

In all scenarios, the addition of firn-aquifer water increased the domain-averaged water pressure and drove formation of persistent channel networks above the ablation zone (Figures 2–3). The firn aquifer exerted this influence despite contributing only ~10% of the total water input to the basal system: the low-elevation inputs supplied ~90% of the subglacial water (Figure 2e).

3.3 Subglacial residence time

We examine subglacial efficiency using the bulk residence time of subglacial water, calculated as the total volume of water in the subglacial system divided by the outflux at the grounding line (Dingman, 2002). In each model scenario, subglacial residence time reached melt-season minima of 10–15 days and winter maxima of 2–3 years (Figures 3f; S9). In the low-elevation and seasonal-ramp scenarios, summer residence time had no multi-year trend. In the other firn-aquifer scenarios, summer residence time decreased by ~10 days, or ~40% (Figures 3f; S8; S9), and winter residence time decreased by >1 year, or ~50–60%. In all seasons except autumn, the addition of meltwater at high elevations decreased the subglacial residence time by Year 4 (Figure S9); however, after firn-aquifer water inputs ceased, residence times recovered to Year 1 values.

4. Discussion

4.1 Effects of a persistent melt supply

The firn-aquifer drainage scenarios increased the volume of water provided to the subglacial system by just 10% but supplied it at higher elevations and at a more uniform rate than the standard low-elevation inputs. Our results indicate that persistent delivery of this inland meltwater to the bed can affect two primary changes in subglacial water pressure: an increase at high-elevations and a decrease at low elevations (Figures 3; S7; Video S1), due to greater longevity of the channel network (Figure 2a–e). Together, these changes accelerate the flow of subglacial water to the ocean.

4.2 Inland subglacial systems and ice velocities

The behavior of the subglacial hydrologic system at inland locations is incompletely understood (Nienow et al., 2017). Observations in western Greenland show clear year-to-year variations in summer ice velocities (Bartholomew et al., 2011a) without substantial variation in annual local

downglacier ice displacement (Tedstone et al., 2015), suggesting sparser subglacial channels and less hydrological efficiency there. Inland channel formation may be limited by a small supply of meltwater to the bed (Bartholomew et al., 2011b; Poinar et al., 2015), and generally shallow bed and surface slopes (Meierbachtol et al., 2013; Dow et al., 2014) in western Greenland.

Our results show that inland channels can form and persist, even in areas with low slopes, if the inland subglacial system receives steady inputs outside the melt season (Figure 2); firn aquifers in eastern Greenland may provide such a water supply. We find that the smaller cross-sectional areas of these inland channels limit their ability to reduce inland water pressure (Figures 3; S8; Video S1). This effect is highlighted by results from the short-ramp and seasonal scenarios: firn-aquifer water drives inland channelization (Figure 2d), but subglacial efficiency grows slowly (~9 months) and the overall inland and moderate-elevation water pressure remain elevated (Figure 3d). These higher subglacial pressures may increase the annual advection of ice at these locations, as has been observed in western Greenland (Doyle et al., 2014), despite fundamentally different supraglacial drainage patterns.

4.3 Subglacial systems and ice velocities of outlet glaciers

In our modeled system, firn-aquifer water input outside the melt season maintains subglacial channels at low elevations over multiple years (Figure 2). Over each subsequent melt season, these inherited channels facilitate more rapid and extensive channel development. Persistent subglacial channels more readily grow to accommodate available meltwater, limiting the early-melt-season increase in subglacial water pressure. We observed this near the terminus, particularly in the firn-aquifer step, long ramp, and short ramp runs (Figure S7). Lower water pressures near the terminus can manifest as increased basal traction (Iken, 1981; Kamb, 1987), which can reduce ice velocities and may encourage terminus retreat (Hewitt, 2017). Overall, our results suggest that the spring speedup often seen in western Greenland on ice overlying distributed drainage systems (e.g., Bartholomew et al., 2011a, Hoffman et al., 2011) may be dampened in areas downstream of draining firn aquifers.

The persistence of channels through the winter decreased wintertime water residence times in the subglacial system in certain firn-aquifer drainage scenarios (Figures 3f; S8). During melt seasons, however, the addition of firn-aquifer water inputs caused greater changes in channel volume than in residence time (Figure S8). We interpret this as evidence that formation of new, inland subglacial channels may have limited utility for evacuating inland water during the melt season. Thus, melt-season efficiency appears to be driven primarily by development of the low-elevation subglacial channel network, but year-round efficiency of this low-elevation network can be increased by addition of high-elevation water sources and development of the inland subglacial network (Figures 3f; S7). A more seasonally persistent subglacial drainage system should pair with more temporally uniform ice velocities; thus, summer velocity variations should be dampened on glaciers where draining firn aquifers feed the subglacial system upstream.

Moon et al. (2014) observed that many Southeast Greenland glaciers show abrupt melt-season speedups followed by late-summer decelerations, but that glaciers in the Ikertivaq region, ~100 km south of Helheim Glacier, had more seasonally consistent speeds. Extensive firn aquifers line the upstream catchments of these glaciers (Miège et al., 2016), making them similar to our idealized Southeast Greenland glacier system. Although we do not model Ikertivaq glaciers specifically, their geometries are consistent with our model setup, and the observed velocity patterns are consistent with our model results: firn-aquifer water supplied to the ice-bed interface should maintain small channels year-round at low elevations (Figure 3), allowing seasonal meltwater to be accommodated more quickly into the subglacial system (Figure 2), and limiting the magnitude of seasonal velocity fluctuations (e.g., Schoof, 2010).

4.4 The role of firn aquifers in ice-sheet mass balance

Our results show the potential for a draining firn aquifer to maintain an active subglacial hydrologic system tens of kilometers upstream from a glacier terminus. The position and drainage times of firn aquifers may allow disproportionately large influence on subglacial hydrology, even in near-terminus regions, despite drainage volumes generally smaller than supraglacial lakes (Poinar et al., 2017). As the extent of Greenland firn-aquifer water increases, drainage events may be more frequent, higher-volume, or occur farther inland, further expanding the potential effect of firn-aquifer drainage on ice flow (Miège et al., 2016; Steger et al., 2017a).

Substantial progress has been made recently in incorporating firn aquifers into surface mass balance models for the Greenland Ice Sheet (e.g., Langen et al., 2017; Ligtenberg et al., 2011; Steger et al., 2017b). In these models, liquid water can flow and accumulate, but is ultimately confined to the firn zone and thus still isolated from the subglacial hydrologic system. Given the demonstrated effects of firn-aquifer drainage on subglacial hydrology and thus the potential to affect ice dynamics, firn aquifers should be included in future considerations of subsurface and subglacial hydrology and, eventually, calculations of dynamically driven ice-sheet mass balance.

5. Conclusion

We demonstrate that water draining from firn aquifers can substantially alter the seasonal behavior of the hydrologic system under an outlet glacier. Firn-aquifer water can create long-lived channels nearly as far upstream as the water input site. These channels, however, cannot accommodate all the meltwater, so firn-aquifer water generally increases the water pressure in the upper part of the model domain. The persistent, overwintered subglacial channels that the firn-aquifer water forms, however, facilitate rapid channel growth downglacier during the melt season, dampening seasonal water pressure variations, shortening the residence time of water in the subglacial system, and lowering subglacial water pressures, especially downglacier,

compared to systems without firn-aquifer inputs. Overall, these lower pressures could moderate seasonal fluctuations in downglacier ice velocities such as those observed on outlet glaciers in the Ikertivaq region of Southeast Greenland.

Overall, the modeled changes to the subglacial hydrologic system are both persistent and widespread, despite the limited amount of water (+10%) added by firn-aquifer drainage. These results underscore the importance of constraining the timing and volume of meltwater release from firn aquifers to our understanding of the subglacial and ice dynamical response to climate change in Greenland.

Acknowledgements

All three authors contributed equally to this work. K.P. was supported by an appointment to the NASA Postdoctoral Program at NASA Goddard Space Flight Center, administered by Universities Space Research Association, and by the Research and Education in eNergy, Environment and Water (RENEW) Institute. L.C.A. acknowledges support from the Global Modeling and Assimilation Office at NASA Goddard Space Flight Center funded under the NASA Modeling, Analysis, and Prediction (MAP) program. C.F.D. was supported by the Canada Research Chairs Programme and the Natural Sciences and Engineering Research Council of Canada. The model simulations were performed using resources provided by Compute Canada. We thank Mauro Werder for use of the GlaDS model, Sophie Nowicki for discussions, and two anonymous reviewers for useful constructive criticism. Model data are available at http://hdl.handle.net/10477/79241.

Figures and captions

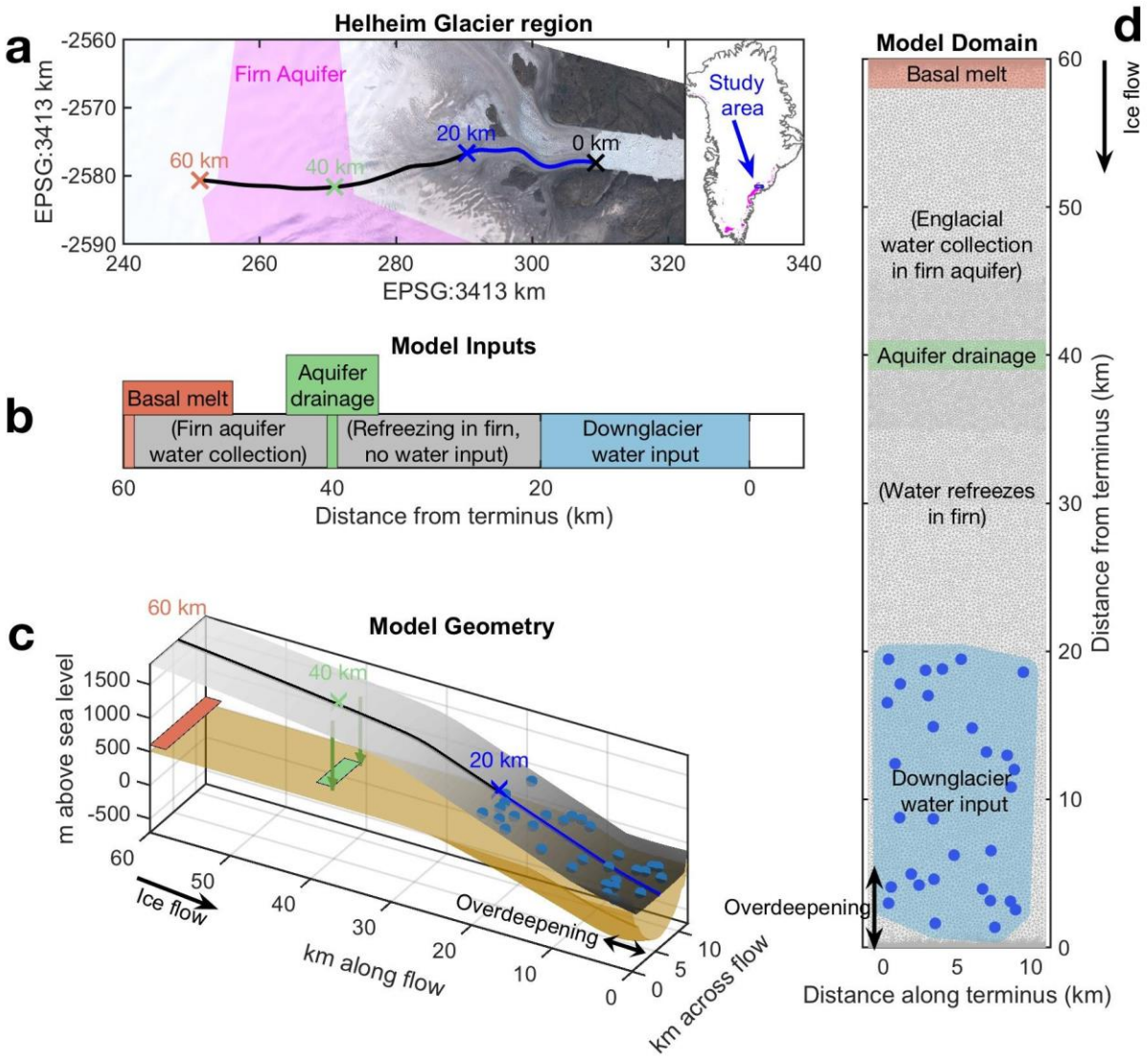

Figure 1

The idealized model domain. (a) Map view of Helheim Glacier, with 3 August 2016 Landsat image. The model domain is loosely designed around a subglacial flowpath that connects a high-elevation region where firn-aquifer water reaches the bed (green) to the terminus. Extent of firn aquifer shown in magenta (Miège et al., 2016). (b) Locations of meltwater inputs (colors). (c) Model geometry with idealized basal parabolic trough. (d) Plan view of the model domain, with meltwater inputs colored, and the model mesh in gray.

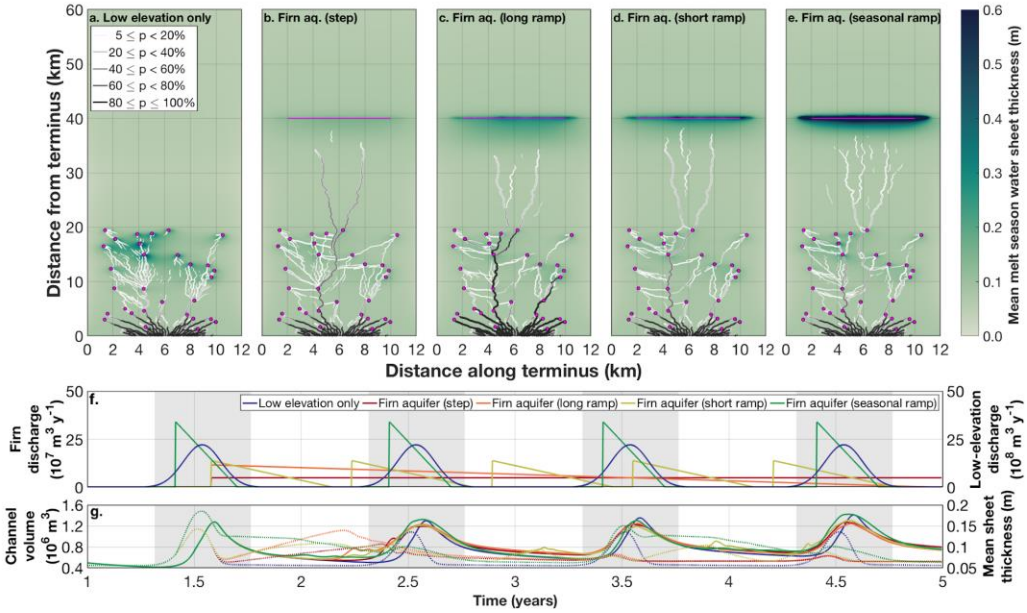

Figure 2

Subglacial sheet thickness and channel persistence for each input scenario. (a) Four-year mean sheet thickness and persistence (*p*) of subglacial channels for the low-elevation scenario. Subglacial channels that persist for 80–100% of model time are indicated in black, with lower persistence values in grays. (b–e) Same as (a), except for firn-aquifer step, long ramp, short ramp, and seasonal ramp scenarios, respectively. Modeled sheet thicknesses in (e) saturates the color scale with a maximum sheet thickness of 2.6 m; (b)–(d) do not saturate. (f) Meltwater input time series for each model scenario. (g) Total subglacial channel volume (solid lines) and domain-averaged water sheet thickness (dotted lines) for each input scenario. Magenta points and lines in (a–e) denote surface melt inputs. Gray bars in (f–g) denote the melt season.

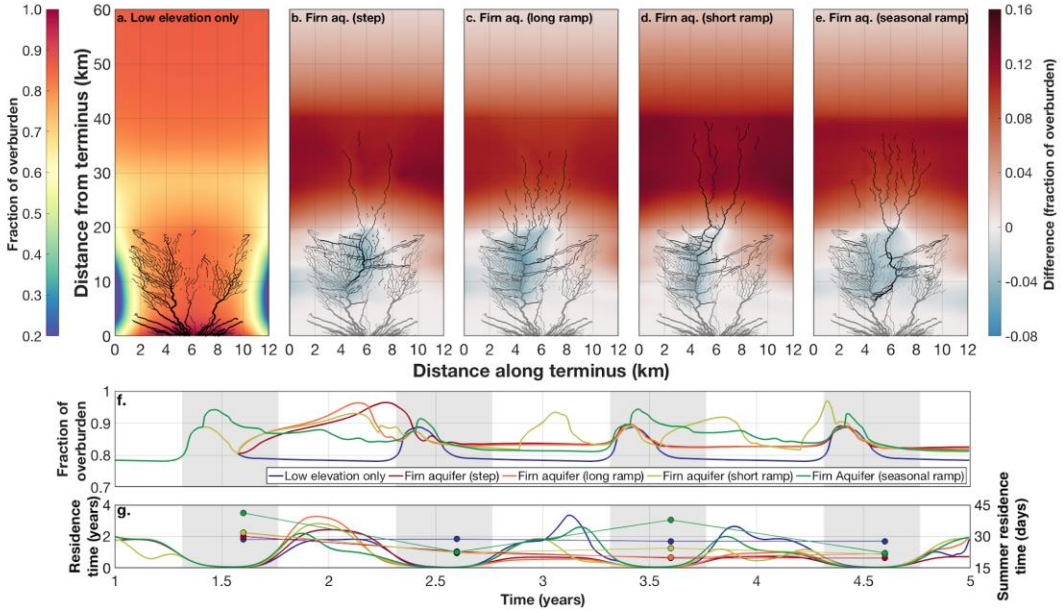

371

372 ## Figure 3

373 Subglacial pressure changes induced by firn-aquifer water input. (a) Four-year mean fraction of
374 overburden pressure (colors) and maximum channel geometry for the low-elevation scenario.
375 (b) Difference in mean water pressure (colors) between the firn-aquifer step and low-elevation
376 runs. Maximum channel extent in firn-aquifer step (black) and low-elevation (gray) runs,
377 showing channels with *c.s.a.* 1–50 m^2. (c)–(e) Same as b, but for firn-aquifer long ramp,
378 seasonal ramp, and short ramp scenarios, respectively. (f) Time series of domain-averaged
379 fraction of overburden water pressure. (g) Time series of subglacial residence time (lines),
380 including the summer (June-July-August) residence time for each year (connected circles). Gray
381 bars in (f–g) denote the melt season.

382

References

Andersen, M. L., Nettles, M., & Elosegui, P. (2011). Quantitative estimates of velocity sensitivity to surface melt variations at a large Greenland outlet glacier. *Journal of Glaciology*, *57*(204), 609–620. doi:10.3189/002214311797409785

Bartholomew, I. D., Nienow, P., Mair, D., Hubbard, A., King, M. A., & Sole, A. (2010), Seasonal evolution of subglacial drainage and acceleration in a Greenland outlet glacier. *Nature Geoscience*, 3(6), 408–411. doi:10.1038/ngeo863

Bartholomew, I., Nienow, P., Sole, A., Mair, D., Cowton, T., Palmer, S., & Wadham, J. (2011a). Supraglacial forcing of subglacial drainage in the ablation zone of the Greenland ice sheet. *Geophysical Research Letters*, *38*(8). doi:10.1029/2011GL047063

Bartholomew, I. D., Nienow, P., Sole, A., Mair, D., Cowton, T., King, M. A., & Palmer, S. (2011b). Seasonal variations in Greenland Ice Sheet motion: Inland extent and behaviour at higher elevations. *Earth and Planetary Science Letters*, *307*(3-4), 271–278. doi:10.1016/j.epsl.2011.04.014

Bevan, S. L., Luckman, A., Khan, S. A. & Murray, T. (2015), Seasonal dynamic thinning at Helheim Glacier. *Earth and Planetary Science Letters*, 415(C), 47–53. doi:10.1016/j.epsl.2015.01.031

Chandler, D. M., Wadham, J. L., Lis, G. P., Cowton, T., Sole, A., Bartholomew, I., et al. (2013). Evolution of the subglacial drainage system beneath the Greenland Ice Sheet revealed by tracers. *Nature Geoscience*, *6*(3), 195–198. doi:10.1038/ngeo1737

Christoffersen, P., M. Bougamont, A. Hubbard, S. H. Doyle, S. Grigsby, & R. Pettersson (2018). Cascading lake drainage on the Greenland Ice Sheet triggered by tensile shock and fracture. *Nature Communications*, *9*(1), 1064. doi:10.1038/s41467-018-03420-8

Clason, C. C., Mair, D., Nienow, P., Bartholomew, I., Sole, A., Palmer, S., & Schwanghart, W. (2015). Modelling the transfer of supraglacial meltwater to the bed of Leverett Glacier, southwest Greenland. *The Cryosphere*, *9*, 123–128. doi:10.5194/tc-9-123-2015

Das, S. B., Joughin, I., Behn, M. D., Howat, I. M., King, M. A., Lizarralde, D., & Bhatia, M. P. (2008). Fracture Propagation to the Base of the Greenland Ice Sheet During Supraglacial Lake Drainage. *Science*, *320*(5877), 778–781. doi:10.1126/science.1153360

Dingman, S. L. (2002). *Physical Hydrology* (2nd ed.). Long Grove, IL: Waveland Press.

Dow, C. F., Werder, M. A., Nowicki, S., & Walker, R. T. (2016). Modeling Antarctic subglacial lake filling and drainage cycles. *The Cryosphere*, *10*, 1318–1393. doi:10.5194/tc-10-1381-2016

Dow, C. F., Karlsson, N. B., and Werder, M. A. (2018), Limited impact of subglacial supercooling freeze-on for Greenland Ice Sheet stratigraphy. *Geophysical Research Letters*, 1–29. doi:10.1002/2017GL076251.

Doyle, S. H., Hubbard, A., & Fitzpatrick, A. (2014). Persistent flow acceleration within the interior of the Greenland ice sheet. *Geophysical Research Letters*, *41*, 899–905. doi:10.1002/2013GL058933

Everett, A., Murray, T., Selmes, N., Rutt, I. C., Luckman, A., James, T. D., et al. (2016). Annual down-glacier drainage of lakes and water-filled crevasses at Helheim Glacier, southeast Greenland. *Journal of Geophysical Research: Earth Surface,* 1–15. doi:10.1002/(ISSN)2169-9011

Fettweis, X., Franco, B., Tedesco, M., van Angelen, J. H., Lenaerts, J. T. M., van den Broeke, M. R., & Gallée, H. (2013). Estimating the Greenland ice sheet surface mass balance contribution to future sea level rise using the regional atmospheric climate model MAR. *The Cryosphere*, *7*(2), 469–489. doi:10.5194/tc-7-469-2013

Forster, R. R., Box, J. E., van den Broeke, M. R., Miège, C., Burgess, E. W., van Angelen, J. H., et al. (2014). Extensive liquid meltwater storage in firn within the Greenland ice sheet. *Nature Geoscience*, *7*, 95–98. doi:10.1038/ngeo2043

Fried, M. J., Catania, G. A., Bartholomaus, T. C., Duncan, D., Davis, M., Stearns, L. A., et al. (2015). Distributed subglacial discharge drives significant submarine melt at a Greenland tidewater glacier. *Geophysical Research Letters*, *42*(21), 9328–9336. doi:10.1002/2015GL065806

Gelaro, R., McCarty, W., Suarez, M. J., Todling, R., Molod, A., Takacs, L., et al. (2017). The Modern-Era Retrospective Analysis for Research and Applications, Version 2 (MERRA-2). *Journal of Climate*, *30*(14), 5419–5454. doi:10.1175/jcli-d-16-0758.1

Hewitt, I. J. (2013). Seasonal changes in ice sheet motion due to melt water lubrication. *Earth and Planetary Science Letters*, *371-372*, 16–25. doi:10.1016/j.epsl.2013.04.022

Hewitt, I. J. (2017). Hydrologically-induced slow-down as a mechanism for tidewater glacier retreat. *EGU General Assembly Conference Abstracts*.

Hoffman, M. J., Catania, G. A., Neumann, T. A., Andrews, L. C., & Rumrill, J. A. (2011). Links between acceleration, melting, and supraglacial lake drainage of the western Greenland Ice Sheet. *Journal of Geophysical Research: Solid Earth*, *116*(F4). doi:10.1029/2010JF001934

Iken, A. (1981). The Effect of the Subglacial Water Pressure on the Sliding Velocity of a Glacier in an Idealized Numerical Model. *Journal of Glaciology*, *27*(97), 407–421. doi:10.3189/S0022143000011448

Kamb, B. (1987). Glacier surge mechanism based on linked cavity configuration of the basal water conduit system. *Journal of Geophysical Research*, 9083–9100.

Kehrl, L., I. Joughin, D. E. Shean, D. Floricioiu, & L. Krieger (2017). Seasonal and interannual variability in terminus position, glacier velocity, and surface elevation at Helheim and Kangerlussuaq Glaciers from 2008 to 2016. *Journal of Geophysical Research*, 122(9), 1635-1652. doi:10.1002/2016JF004133

Kuipers Munneke, P., Ligtenberg, S. R. M., van den Broeke, M. R., van Angelen, J. H., & Forster, R. R. (2014). Explaining the presence of perennial liquid water bodies in the firn of the Greenland Ice Sheet. *Geophysical Research Letters*. doi:10.1002/(ISSN)1944-8007

Lampkin, D. J., & VanderBerg, J. (2013). Supraglacial melt channel networks in the Jakobshavn Isbrae region during the 2007 melt season. *Hydrological Processes*. doi:10.1002/hyp.10085

Langen, P. L., Fausto, R. S., Vandecrux, B., Mottram, R. H., & Box, J. E. (2017). Liquid Water Flow and Retention on the Greenland Ice Sheet in the Regional Climate Model HIRHAM5: Local and Large-Scale Impacts. *Frontiers in Earth Science*, *4*, 61–18. doi:10.3389/feart.2016.00110

Legchenko, A., C. Miège, L. S. Koenig, R. R. Forster, O. Miller, D. K. Solomon, N. Schmerr, L. Montgomery, S. Ligtenberg, & L. Brucker (2018). Estimating water volume stored in the south-eastern Greenland firn aquifer using magnetic-resonance soundings. *Journal of Applied Geophysics*. doi:10.1016/j.jappgeo.2018.01.005

Ligtenberg, S. R. M., Helsen, M. M., & van den Broeke, M. R. (2011). An improved semi-empirical model for the densification of Antarctic firn. *The Cryosphere*, *5*(4), 809–819. doi:10.5194/tc-5-809-2011

Machguth, H., MacFerrin, M., Van As, D., Box, J. E., Charalampidis, C., Colgan, W., et al. (2016). Greenland meltwater storage in firn limited by near-surface ice formation. *Nature Climate Change*, *6*(4), 390–393. doi:10.1038/nclimate2899

McGrath, D., Colgan, W., Bayou, N., Muto, A., & Steffen, K. (2013). Recent warming at Summit, Greenland: Global context and implications, *40*(10), 2091–2096. doi:10.1002/grl.50456

Meierbachtol, T., Harper, J., & Humphrey, N. (2013). Basal Drainage System Response to Increasing Surface Melt on the Greenland Ice Sheet. *Science*, *341*(6147), 777–779. doi:10.1126/science.1235905

Miège, C., Forster, R. R., Brucker, L., Koenig, L. S., Solomon, D. K., Paden, J. D., et al. (2016). Spatial extent and temporal variability of Greenland firn aquifers detected by ground and airborne radars. *Journal of Geophysical Research*, 1–45. doi:10.1002/2016jf003869

485 Miller, O. L., D. K. Solomon, C. Miège, L. Koenig, R. Forster, N. Schmerr, S. R. M. Ligtenberg,
486 and L. Montgomery (2017), Direct evidence of meltwater flow within a firn aquifer in
487 Southeast Greenland, *Geophysical Research Letters*, 1–15, doi:10.1002/2017GL075707.

488 Moon, T., Joughin, I., Smith, B., Broeke, M. R., Berg, W. J., Noël, B., & Usher, M. (2014).
489 Distinct patterns of seasonal Greenland glacier velocity. *Geophysical Research Letters*,
490 *41*(20), 7209–7216. doi:10.1002/2014GL061836.

491 Mottram, R., Boberg, F., Langen, P., Yang, S., Rodehacke, C., Christensen, J. H., & Madsen,
492 M. S. (2017). Surface mass balance of the Greenland ice sheet in the regional climate
493 model HIRHAM5: Present state and future prospects. *Low Temperature Science*, 105–115.
494 doi:10.14943/lowtemsci.75.105

495 Nienow, P. W., Sole, A. J., Slater, D. A., & Cowton, T. R. (2017). Recent Advances in Our
496 Understanding of the Role of Meltwater in the Greenland Ice Sheet System. *Current*
497 *Climate Change Reports*, 1–15. doi:10.1007/s40641-017-0083-9

498 Noël, B., van de Berg, W. J., Machguth, H., Lhermitte, S., Howat, I., Fettweis, X., & van den
499 Broeke, M. R. (2016). A daily, 1 km resolution data set of downscaled Greenland ice sheet
500 surface mass balance (1958–2015). *The Cryosphere*, *10*(5), 2361–2377. doi:10.5194/tc-10-
501 2361-2016

502 Parizek, B. R., & Alley, R. B. (2004). Implications of increased Greenland surface melt under
503 global-warming scenarios: ice-sheet simulations. *Quaternary Science Reviews,* 23(9-10),
504 1013–1027. doi:10.1016/j.quascirev.2003.12.024

505 Poinar, K., Joughin, I., Das, S. B., Behn, M. D., Lenaerts, J. T. M., & van den Broeke, M. R.
506 (2015). Limits to future expansion of surface-melt-enhanced ice flow into the interior of
507 western Greenland. *Geophysical Research Letters*, *42*(6), 1800–1807.
508 doi:10.1002/2015GL063192

509 Poinar, K., Joughin, I., Lilien, D., Brucker, L., Kehrl, L., & Nowicki, S. (2017). Drainage of
510 Southeast Greenland Firn Aquifer Water through Crevasses to the Bed. *Frontiers in Earth*
511 *Science*, *5*, 8–15. doi:10.3389/feart.2017.00005

512 Schild, K. M., R. L. Hawley, & B. F. Morriss (2016). Subglacial hydrology at Rink Isbræ, West
513 Greenland inferred from sediment plume appearance. *Annals of Glaciology*, *57*(72), 118–
514 127. doi:10.1017/aog.2016.1.

515 Schoof, C. (2010). Ice-sheet acceleration driven by melt supply variability. *Nature*, *468*(7325),
516 803–806. doi:10.1038/nature09618

517 Shannon, S. R., Payne, A. J., Bartholomew, I. D., van den Broeke, M. R., Edwards, T. L.,
518 Fettweis, X., et al. (2013). Enhanced basal lubrication and the contribution of the Greenland

ice sheet to future sea-level rise. *Proceedings of the National Academy of Sciences,* 110(35), 14156–14161. 10.1073/pnas.1212647110

Smith, L. C., Chu, V. W., Yang, K., Gleason, C. J., Pitcher, L. H., Rennermalm, A. K., et al. (2015). Efficient meltwater drainage through supraglacial streams and rivers on the southwest Greenland ice sheet. *Proceedings of the National Academy of Sciences of the United States of America*, 112(4), 1001–1006. doi:10.1073/pnas.1413024112

Steger, C. R., Reijmer, C. H., & van den Broeke, M. R. (2017a). The modelled liquid water balance of the Greenland Ice Sheet. *The Cryosphere Discussions*, 1–32. doi:10.5194/tc-2017-88

Steger, C. R., Reijmer, C. H., van den Broeke, M. R., Wever, N., Forster, R. R., Koenig, L. S., et al. (2017b). Firn Meltwater Retention on the Greenland Ice Sheet: A Model Comparison. *Frontiers in Earth Science*, *5*, F03011–16. doi:10.3389/feart.2017.00003

Straneo, F., Curry, R. G., Sutherland, D. A., Hamilton, G. S., Cenedese, C., Våge, K., & Stearns, L. A. (2011). Impact of fjord dynamics and glacial runoff on the circulation near Helheim Glacier. *Nature Geoscience*, *4*(5), 322–327. doi:10.1038/ngeo1109

Sundal, A. V., Shepherd, A., Nienow, P., Hanna, E., Palmer, S., & Huybrechts, P. (2011), Melt-induced speed-up of Greenland ice sheet offset by efficient subglacial drainage, *Nature*, 469(7331), 521–524. doi:10.1038/nature09740

Tedstone, A. J., P. W. Nienow, P.W., Gourmelen, N., Dehecq, A., Goldberg, D., and Hanna, E. (2015), Decadal slowdown of a land-terminating sector of the Greenland Ice Sheet despite warming, *Nature*, 526(7575), 692–695. doi:10.1038/nature15722

Werder, M. A., Hewitt, I. J., Schoof, C. G., & Flowers, G. E. (2013). Modeling channelized and distributed subglacial drainage in two dimensions, *Journal of Geophysical Research: Earth Surface*, 118(4), 2140–2158. doi:10.1002/jgrf.20146

Additional References – Supporting Information

Aschwanden, A., Bueler, E., Khroulev, C. & Blatter, H. (2012), An enthalpy formulation for glaciers and ice sheets, *Journal of Glaciology*, *58*(209), 441–457, doi:10.3189/2012JoG11J088

Banwell, A. F., Willis, I. C. & Arnold, N. S. (2013), Modeling subglacial water routing at Paakitsoq, W Greenland, *Journal of Geophysical Research: Earth Surface*, 118(3), 1282–1295, doi:10.1002/jgrf.20093

de Fleurian, B. et al. (2018), SHMIP: The Subglacial Hydrology Model Intercomparison Project, *Journal of Glaciology*, 467, 1–20, doi:10.1017/jog.2018.78

552 Dow, C. F. et al. (2015). Modeling of subglacial hydrological development following rapid
553 supraglacial lake drainage. *Journal of Geophysical Research: Earth Surface*, *120*(6), 1127–
554 1147. doi:10.1002/2014jf003333

555 Doyle, S. H., Hubbard, A. L., Dow, C. F., Jones, G. A., Fitzpatrick, A., Gusmeroli, A., et al.
556 (2013). Ice tectonic deformation during the rapid in situ drainage of a supraglacial lake on
557 the Greenland Ice Sheet. *The Cryosphere*, *7*(1), 129–140. doi:10.5194/tc-7-129-2013

558 Howat, I., Negrete, A. & Smith, B. E. (2014). The Greenland Ice Mapping Project (GIMP) land
559 classification and surface elevation data sets. *The Cryosphere*, 8(4), 1509–1518.
560 doi:10.5194/tc-8-1509-2014

561 Howat, I., Negrete, A. & Smith, B. (2015). *MEaSUREs Greenland Ice Mapping Project (GIMP)*
562 *Digital Elevation Model, Version 1*. Boulder, Colorado USA. NASA National Snow and Ice
563 Data Center Distributed Active Archive Center. doi:10.5067/NV34YUIXLP9W

564 MacGregor, J. A., Fahnestock, M. A., Catania, G. A., Aschwanden, A., Clow, G. D., Colgan, W.
565 T., et al. (2016). A synthesis of the basal thermal state of the Greenland Ice Sheet. *Journal*
566 *of Geophysical Research: Earth Surface*, 1–44. doi:10.1002/2015JF003803

567 Morlighem, M., E. Rignot, J. Mouginot, H. Seroussi, and E. Larour (2014). Deeply incised
568 submarine glacial valleys beneath the Greenland ice sheet, *Nature Geoscience*, 7(6), 418–
569 422, doi:10.1038/ngeo2167

570 Morlighem, M., Williams, C., Rignot, E., An, L., Arndt, J. E., Bamber, J., et al. (2017a).
571 BedMachine v3: Complete bed topography and ocean bathymetry mapping of Greenland
572 from multi-beam echo sounding combined with mass conservation, *Geophysical Research*
573 *Letters*, 44, doi:10.1002/2017GL074954

574 Morlighem, M. et al. (2017b). *IceBridge BedMachine Greenland, Version 3*. Boulder, Colorado
575 USA. NASA National Snow and Ice Data Center Distributed Active Archive Center.
576 doi:10.5067/2CIX82HUV88Y

577 Phillips, T., Leyk, S., Rajaram, H., Colgan, W., Abdalati, W., McGrath, D. & Steffen, K. (2011),
578 Modeling moulin distribution on Sermeq Avannarleq glacier using ASTER and WorldView
579 imagery and fuzzy set theory, *Remote Sensing of the Environment*, 115(9), 2292–2301,
580 doi:10.1016/j.rse.2011.04.029

581 Wei, W., Greenbaum, J. S., Gourmelen, N., Dow, C. F., Bo, S., Guo, J., van Ommen, T. D.,
582 Roberts, J. L., Young, D. A., and Blankenship, D. D. (2018). The bathymetric and subglacial
583 hydrological context for basal melting of the West Ice Shelf in East Antarctica. AGU Fall
584 Meeting, 11 December 2018, San Francisco, C21C-1355

Geophysical Research Letters

Supporting Information for

Long-term maintenance of an active subglacial hydrologic system in Southeast Greenland by firn aquifers

Kristin Poinar[1], Christine F. Dow[2], Lauren C. Andrews[3]
[1]University at Buffalo, [2]University of Waterloo, [3]NASA Goddard Space Flight Center

Contents of this file

Additional Supporting Information (Files uploaded separately)

Supplemental Text: Methods

ST.1 GlaDS model

We implemented the Glacier Drainage System (GlaDS) model, a 2D finite element model for coupled distributed and channelized subglacial drainage (Werder et al., 2013; Dow et al., 2016). The distributed components in GlaDS evolve on elements of an unstructured mesh through the balance of sliding-driven cavity opening and creep closure. Subglacial channels develop along element edges through melt into the overlying ice, driven by viscous heat dissipation. The model prescribes equal subglacial pressures across any subglacial channel and its adjacent distributed sheet, allowing exchange between the two components at nodes of the mesh. The model uses an adaptive time-stepping routine and, for these experiments, has a 3-day output interval.

Table S1. Values of parameters used in the GlaDS model.

Parameter	Value	Units
Ice flow constant	2.5×10^{-25}	$Pa\cdot s^{-1}$
Glen's flow law exponent	3	-
Gravitational acceleration	9.81	$m\cdot s^{-2}$
Latent heat of fusion	3.34×10^{-5}	$J\cdot kg^{-1}$
Ice density	910	$kg\cdot m^{-3}$
Water density	1000	$kg\cdot m^{-3}$
Englacial void ratio	1×10^{-5}	-
Basal sliding speed	≤ 800	$m\cdot yr^{-1}$
Bedrock bump height	0.08	m
Cavity spacing	2	m
Sheet conductivity	1×10^{-4}	$m^{7/4}\cdot kg^{-1/2}$
Sheet width below channel	2	m
Channel conductivity	5×10^{-2}	$m^{3/2}\cdot kg^{-1/2}$
Upstream boundary flux	694	$m^{2}\cdot yr^{-1}$
Basal melt rate	0.02	$m\cdot yr^{-1}$

The GlaDS model has been used to simulate the development of the subglacial hydrologic system in alpine-type glaciers (Werder et al., 2013), the interior of the Greenland Ice Sheet (Dow et al, 2018), and Antarctic subglacial lakes and hydrology (Dow et al., 2016, 2018). The model is detailed in full in Werder et al. (2013) and summarized in Dow et al. (2016). Parameters specific to the results presented here are included in Table S1.

ST.1.1 Model sensitivity to parameters

In addition to application to subglacial hydrology in alpine, Antarctic, and Greenlandic settings (Werder et al, 2013; Dow et al 2016; Dow et al 2018; Downs et al 2018), GlaDS has participated as a primary model in the Subglacial Hydrology Model Intercomparison Project (SHMIP; de Fleurian et al, 2018). As such, GlaDS has undergone a range of sensitivity tests and the sensitivity of model results to most individual parameters is well constrained. However, it should be noted that the exact subglacial conditions at any given site are unconstrained; therefore, in this study, we use best-estimate parameter choices and keep them constant among all model runs.

As demonstrated in Werder et al (2013) and Dow et al (2016), the sheet conductivity, basal bedrock bump height, and cavity spacing all interact with the water input rate to determine when the system becomes pressurized and by how much. If these values are higher than is realistic, the system will often stay at steady state and will not fully pressurize. Similarly, in the opposite scenario, the system will excessively pressurize and become unstable. As such, a well-chosen combination of these three parameters is necessary for intermediate pressurization. In the absence of independent subglacial hydrology data, we apply the standard values for these parameters of 10^{-4} $m^{7/4} \cdot kg^{-1/2}$ sheet conductivity, 2 m cavity spacing and 0.08 m bedrock bump height (see Dow et al., 2016, 2018). The effect of changing channel conductivity (equivalent to conduit wall roughness) is a subtle difference in channel onset location and channel network arborescence.

When applied to real topography, GlaDS accurately predicts channel location and relative flux over the grounding line, as confirmed by independent ice shelf melt measurements (Wei et al, 2018). Our tests are applied to an idealized study area with synthetic topography, and we seek only to constrain the differences between different input scenarios, so we examine only the relative positions of subglacial channels between runs.

To add to the already published suite of sensitivity test for GlaDS, we ran sensitivity tests for glacier geometry and basal sliding speed. Werder et al. (2013) found that runs with steeper basal topography developed a denser channel network, but that surface topography was a greater control on channel formation. To explore the effects of our melt inputs on channelization, we test two glacier geometries: a flat bed with a uniformly sloping surface, and a basal trough with a mass-conserving surface. The latter geometry is broadly representative of a large outlet glacier but synthetically constructed. We ran the model with these geometries and both low-elevation and firn-aquifer step inputs. The topographic, ice thickness, and ice speed differences result in a mean difference in fraction of overburden of -0.035 (basal trough minus flat bed) and a maximum difference of 1.3 (basal trough minus flat bed), as shown in Figure S10. The spatial pattern of

mean differences is strongly driven by the curvature of the bed, with the largest pressure differences located at the low-elevation margins, where differences in ice thickness are greatest (Figure S10a–b). These differences in overburden pressure change the channel orientation, but do not substantially change the maximum length or size of the channels (Figure S10c–d). Mean changes in sheet thickness are also minor (-0.009 m; basal trough minus laterally flat bed), with the maximum difference being -0.5 m (basal trough minus laterally flat bed). These differences arise due to local differences in bed slope, which encourage faster advection of water, particularly during the summer melt season, to the centerline of the basal trough.

We also studied the sensitivity of the subglacial hydrological system to ice flow speed by capping the ice flow near the outlet-glacier terminus (within 10 km) to 500 $m \cdot y^{-1}$ and 800 $m \cdot y^{-1}$ and running the low-elevation input and firn aquifer step inputs. Over the majority of the model domain, the ice flow speed did not change between these cases. Results are shown in Figures S11–12. With low-elevation water inputs, there is a mean fraction of overburden difference of -0.001 (800 $m \cdot y^{-1}$ run minus 500 $m \cdot y^{-1}$ run) and a maximum difference of -0.06; (800 $m \cdot y^{-1}$ run minus 500 $m \cdot y^{-1}$ run). The differences in maximum value clearly change signs ~10 km from the terminus where the velocity cap is enforced; however, these differences are only present during the onset of the melt season and have very limited effect on subglacial pressures and channel location persistence (Figure S11). With firn-aquifer step inputs, there are reasonable differences between the 800 $m \cdot y^{-1}$ and 500 $m \cdot y^{-1}$ runs, primarily due to a slight lateral shift (~1 km) in the location of an 8-km reach of the main drainage channel (Figure S12d). Overall, this shift causes a very limited change in the field-mean fraction of overburden (-0.0004; 800 $m \cdot y^{-1}$ minus 500 $m \cdot y^{-1}$). Though these differences are clearly visible during the melt season (max: 0.46; 800 $m \cdot y^{-1}$ minus 500 $m \cdot y^{-1}$). These maximum changes in pressure are due to changes in the relative location of input locations to developed subglacial channels, as indicated by the maximum sheet thicknesses and subglacial channel persistence (max difference: -0.6 m; Figure S12d), but are limited in the time-mean field (mean difference: 0.002 m; Figure S12c).

While there can be locally large differences between model runs with different bed geometries and maximum ice velocities, these differences are localized in both space and time, resulting in only small differences over the duration of the model runs (Figures S10–S12). We have selected the parameters that best reflect the outlet glaciers located downstream of firn aquifers: basal trough geometry and higher (800 $m \cdot yr^{-1}$) ice velocity cap. Since our primary goal is intercomparison of model runs with and without firn-aquifer inputs, the small sensitivities presented here would not substantially alter the presented interpretation.

ST.2 Model domain

The model domain is 60 km long and 12 km wide. The top 30 km of the domain has a flat bed with slope 0.0017 and a parabolic surface that initiates at s = 1800 m above sea level (a.s.l.). Ice thickness is 1300 m at the top of the domain and decreases to 925 m as the surface lowers parabolically. At 30 km from the upstream end of the domain, the bed opens into a smooth, symmetric trough that descends from 0 meters a.s.l. to -680 meters at its lowest central point at

a uniform slope of 46 meters per kilometer (-0.046). The trough contains an overdeepening in the 8 km upstream of the terminus. The lateral shape of the trough is loosely based on the geometry of the southern branch of Helheim Glacier just upstream of where it joins the main trough, ~15 km from the terminus. We started with the Morlighem et al. (2014) transect at this point, stretched its width (~5 km) to fit our 12-km-wide domain, smoothed it with a 1-km pseudo-Gaussian filter, and averaged the results across the centerline to make a symmetric geometry. Finally, we repeated this lateral shape, with vertical scaling ranging from 0 m (no trough) to -680 m (at its deepest point), from 30 km upstream of the terminus to 4 km upstream of the terminus at the center of the overdeepening, respectively. The final 4 km of the bedrock rise out of the overdeepening, reaching -550 m above sea level at the center of the trough at the terminus.

The ice-sheet surface is also loosely based on the surface profile of Helheim Glacier near its confluence point; again, we widened the Morlighem et al. (2014) transect at this location to 12 km, smoothed it with a 4-km pseudo-Gaussian filter, and averaged the results across the centerline. We scaled this lateral shape down the flowline such that the ice thickness remained constant, at 925 meters, above the trough centerline. Near the edges, the surface is set such that the minimum ice thickness is 200 meters.

The upper half of the model domain features gently sloping terrain typical of elevations where firn aquifers form. We designed the steeply sloping, incised trough in the lower half of the domain to represent a typical outlet glacier, where surface meltwater flows relatively quickly over bare ice and drains directly to the bed (e.g., Everett et al., 2016; McGrath et al., 2011).

We defined the flow field of the ice by applying mass conservation to our model geometry. At the upstream boundary, we prescribed along-glacier ice flow of 100 $m \cdot y^{-1}$ and no lateral ice flow. At the onset of the bedrock trough 30 km upstream of the terminus, we prescribe a quartic ($\sim x^4$) flow profile pinned at 100 $m \cdot y^{-1}$ on the sidewalls, with the centerline velocity dictated by the shape of the bedrock and surface. The ice reaches a maximum along-flow speed of 1 $km \cdot y^{-1}$ at the centerline in the overdeepening. Lateral flow up to 90–100 $m \cdot y^{-1}$ also occurs to fill the trough, especially at the overdeepening. Due to computational limitations associated with the distributed phase in the hydrology model, we cap the ice speed at 800 $m \cdot y^{-1}$. In contrast, ice in Helheim Glacier and other Southeast Greenland glaciers flows at 1–10 km·y-1 (Kehrl et al., 2017; Moon et al., 2014). Figure S13 shows the ice speed used in the model.

ST.3 Subglacial hydrology model setup

We prescribe zero water inflow at the lateral boundaries via Neumann boundary conditions for subglacial water pressure. The upper boundary also has a Neumann condition, but with a fixed flux calculated to represent input from the catchment upstream of the model domain (see next section). We implement a Dirichlet boundary condition at the downstream end of the domain, setting subglacial water pressure equal to ice overburden pressure to represent ocean termination.

We initiate the GlaDS model for our simulations by running it to steady state with a spatially uniform basal water flux of 0.02 $m \cdot yr^{-1}$ prescribed over the entire model domain with no other water inputs. This flux is representative of the basal melt rate (Aschwanden et al., 2012). These inputs drive the development of a subglacial water pressure field that is typical of winter subglacial conditions , with water draining almost fully within a distributed system (small channels form only near the terminus). The domain-averaged subglacial pressure is ~78% of overburden pressure. Water pressure approaches zero toward the sides of the trough and approaches flotation between the overdeepening and the ice front. Upglacier of the trough, water pressure averages 84% of overburden.

We force the model with basal sliding velocities, basal meltwater flux and supraglacial meltwater inputs (Table S1). We approximate downglacier meltwater inputs as point sources, which we input at element nodes, and higher-elevation englacial drainage as line sources, which we input into a fixed set of elements and nodes.

Diurnal variations in meltwater supply enhance the rate of subglacial channelization (Hewitt et al., 2013); in particular, rapid melt events such as supraglacial lake drainages can cause large but short-lived changes in subglacial pressure (Dow et al., 2015) and velocity (Hoffman et al., 2011; Das et al., 2008). To better focus on persistent changes to the subglacial system compared to the wintertime background, we exclude such sub-daily fluctuations in meltwater fluctuations and input meltwater at 3-day resolution. As previously stated, the GlaDS model uses a variable timestep, calculated and implemented internally as necessary.

ST.4 Meltwater supplied to the subglacial system

ST.4.1 Basal meltwater inputs

To represent the basal melt across the subglacial catchment upstream of our model domain, we prescribe a time-invariant water flux across the upstream boundary. We delineate this basin by calculating the subglacial hydropotential of the southern branch of Helheim Glacier from bed (Morlighem et al., 2017a, 2017b) and surface topography (Howat et al., 2014, 2015) and assuming subglacial water pressure equal to overburden pressure. This subglacial drainage basin is approximately 2160 km^2, and the area inland of the 1800-m surface elevation contour, which we use as an approximation to our upstream domain boundary, is 413 km^2. Basal melt occurs across the full extent of this upstream basin (MacGregor et al., 2016). Assuming a uniform basal melt rate of 0.02 $m \cdot yr^{-1}$ (Aschwanden et al., 2012), we estimate a basin-integrated basal melt input of 8.3×10^6 $m^3 \cdot yr^{-1}$, which amounts to a flux of 690 $m^2 \cdot yr^{-1}$ across our 12-km upstream boundary.

ST.4.2 Low-elevation water inputs

We divide the meltwater produced in the lowest 20 km of our model domain evenly among 30 water input sites. We placed these sites randomly in the center 10 km of the outlet glacier, so that no site is within 1 km of the lateral boundaries. This distribution gives a water input site density of

0.125 per square kilometer, similar to observations in the western GrIS ablation zone (Smith et al., 2015; Banwell et al., 2013; Phillips et al, 2011). Locations of low-elevation water inputs are held constant among all model runs.

We calculate the temporal pattern of meltwater fed into these sites by averaging the daily MERRA-2 surface runoff for our study area over 1981–2016, then smoothing these annual curves with a 14-day pseudo-Gaussian (Figure 2e; Gelaro et al., 2017). We verified these input curves against MAR v3.7 melt model output. The total meltwater input amounts to 4.9×10^{8} $m^3 \cdot yr^{-1}$, which we divide evenly among the 30 sites in our lower model domain. The maximum water input through each site in one three-day input step is 2.3 $m^3 \cdot s^{-1}$ on July 16–18 of each year. This value compares well to field measurements of ~0.5–3 $m^3 \cdot s^{-1}$ peak flow rates (McGrath et al., 2011; Meierbachtol et al., 2013).

ST.4.3 High-elevation firn-aquifer water inputs

The temporal pattern of meltwater discharge from the firn aquifer – crevasse system is not well constrained. To account for this uncertainty, we test four scenarios for firn-aquifer water input to the bed, holding the volume of water input to the subglacial system constant across all scenarios. This allows us to isolate the effects of the temporal shape of the input on the basal hydrology (Schoof, 2010).

In western Greenland, lake drainages through kilometer-scale-long crevasses form temporary line sources of water to the bed, which typically collapse into moulins, or point sources, as the water supply slows (Das et al., 2008; Doyle et al., 2013). In Southeast Greenland, firn-aquifer hydrofractures also begin as linear features (line sources) that are at least hundreds of meters long, but the subsurface nature of these conduits makes it difficult to study their evolution (Poinar et al., 2017). It is currently unknown whether firn-aquifer water flow would maintain a line source to the bed, as we model here, or focus water into a smaller zone that would resemble a point source of water to the bed. The effects of such a point-source on the subglacial hydrological system would likely be more spatially limited than the regional effects we find here (Figure 3).

Supplementary Figures

Figure S1. Annually stacked pressure evolution

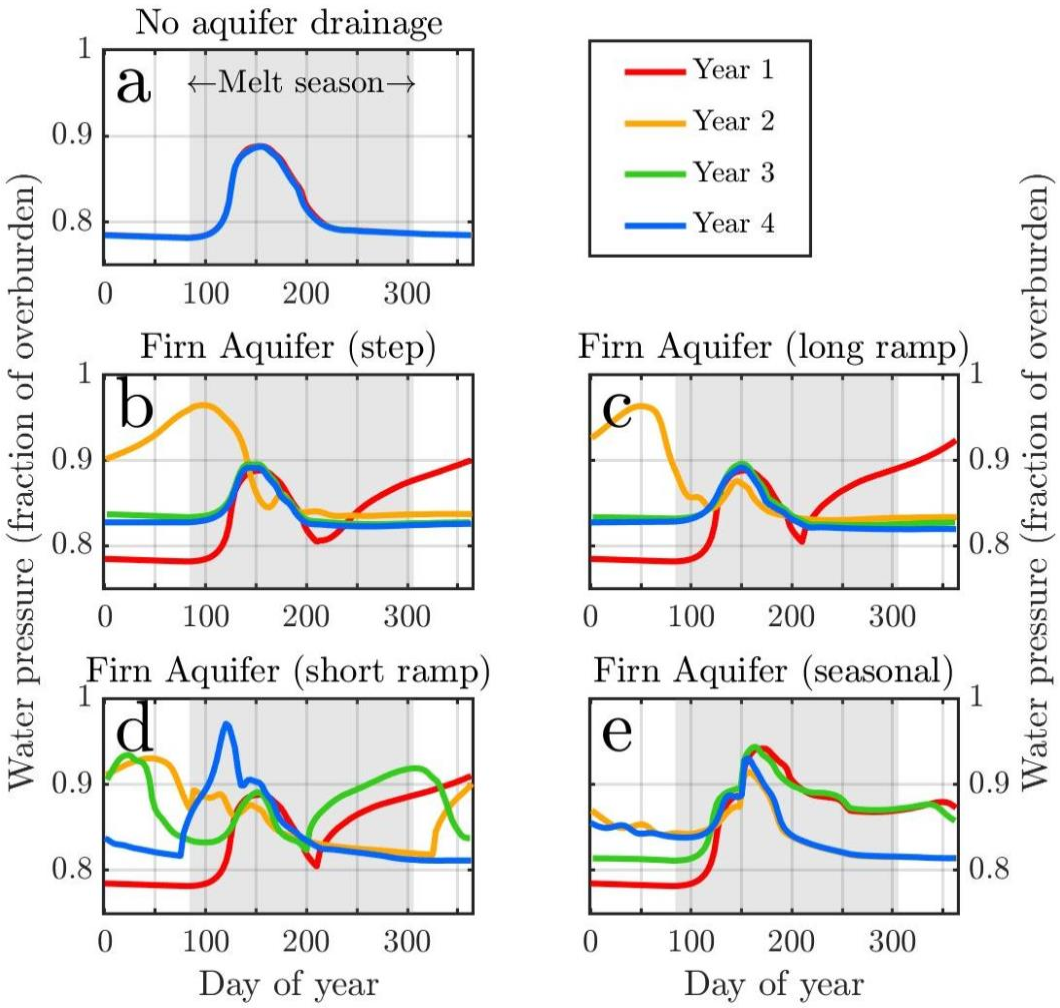

Figure S1. Evolution of the domain-averaged subglacial water pressure over all model runs. Extent of the melt season is shown in gray. Colors indicate the model year; the time series on each panel wrap from right to left (e.g., Day 365 of Year 1 (red) is continuous with Day 1 of Year 2 (orange) for each panel, and so on). The various water input scenarios are shown in panels a–f. The effect of firn-aquifer drainage on the mean subglacial water pressure is seen by comparing to panel a.

Figure S2–6. Annual evolution of subglacial water pressure for each meltwater input scenario

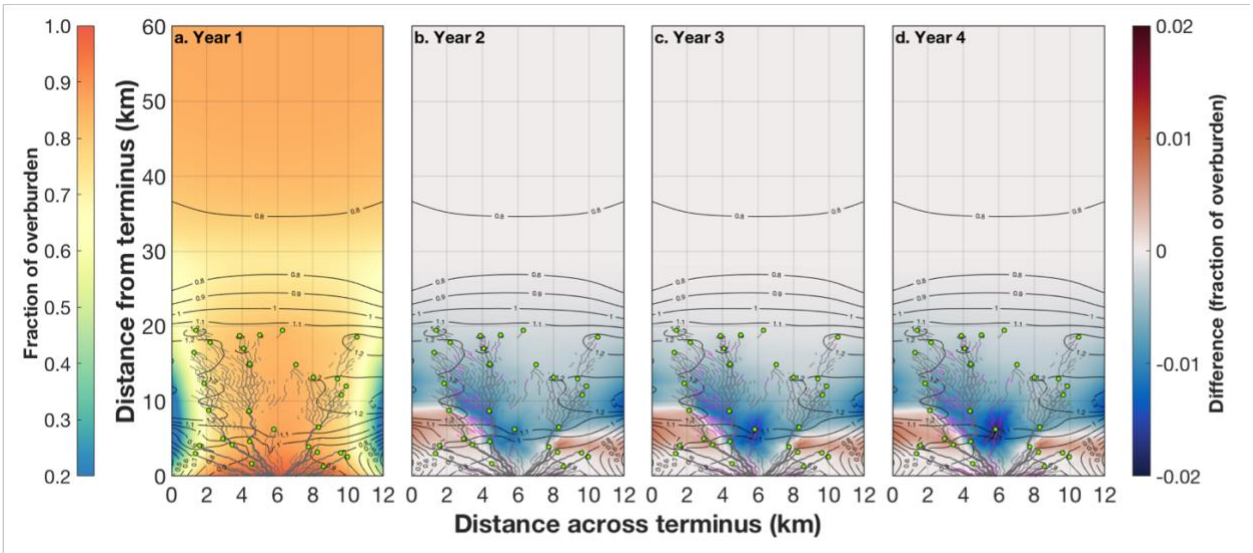

Figure S2. Evolution of subglacial water pressure for the low-elevation scenario, by year. (a) Year 1 mean annual pressure field and maximum channel extent (grey lines). Maximum fraction of overburden in each year indicated by black contours. Low-elevation and firn-aquifer input locations are indicated with green circles or green lines, respectively. (b) Differenced mean annual pressure field (Year 2 minus Year 1) and maximum channel extent for Year 1 (grey lines) and Year 2 (magenta lines). (c) Same as b, except for Year 3. (d) Same as b, except for Year 4.

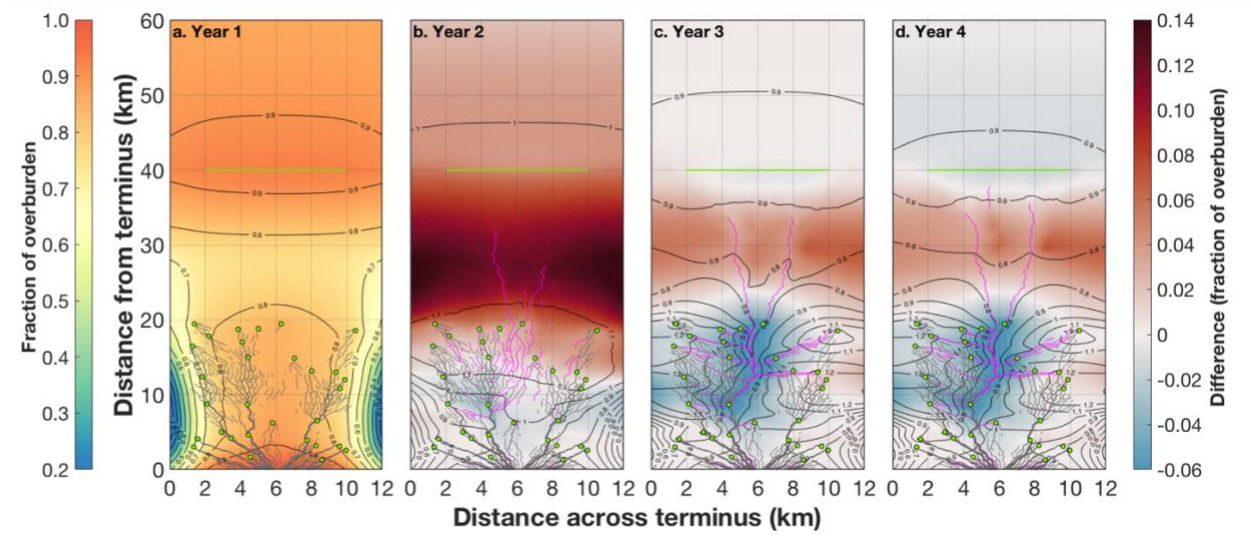

Figure S3. Evolution of subglacial water pressure for the firn aquifer step function run, by year. (a–d) Same as Figure S2, except for the firn aquifer step function input.

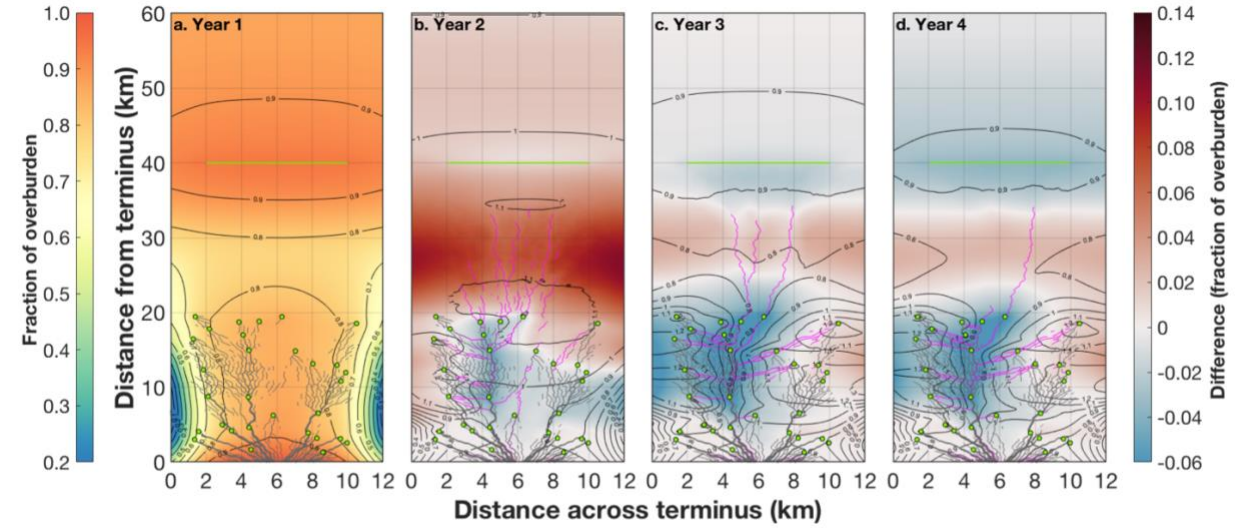

Figure S4.

Evolution of subglacial water pressure for the firn aquifer long ramp run, by year. (a–d) Same as Figure S2, except for the firn aquifer long ramp input.

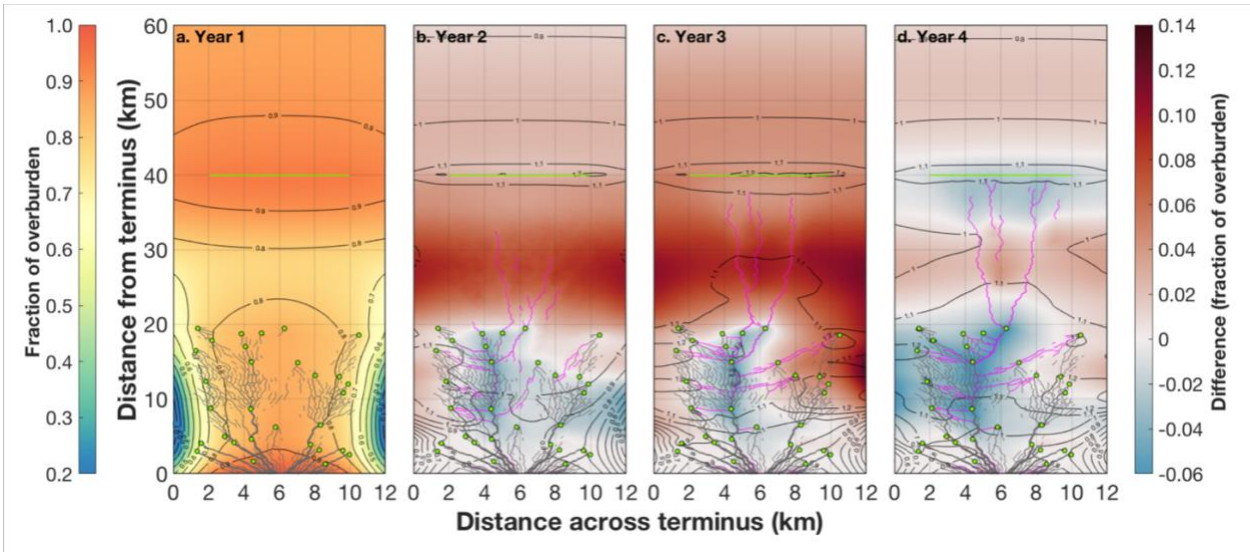

Figure S5. Evolution of subglacial water pressure for the firn aquifer short ramp run, by year. (a–d) Same as Figure S2, except for the firn aquifer short ramp input.

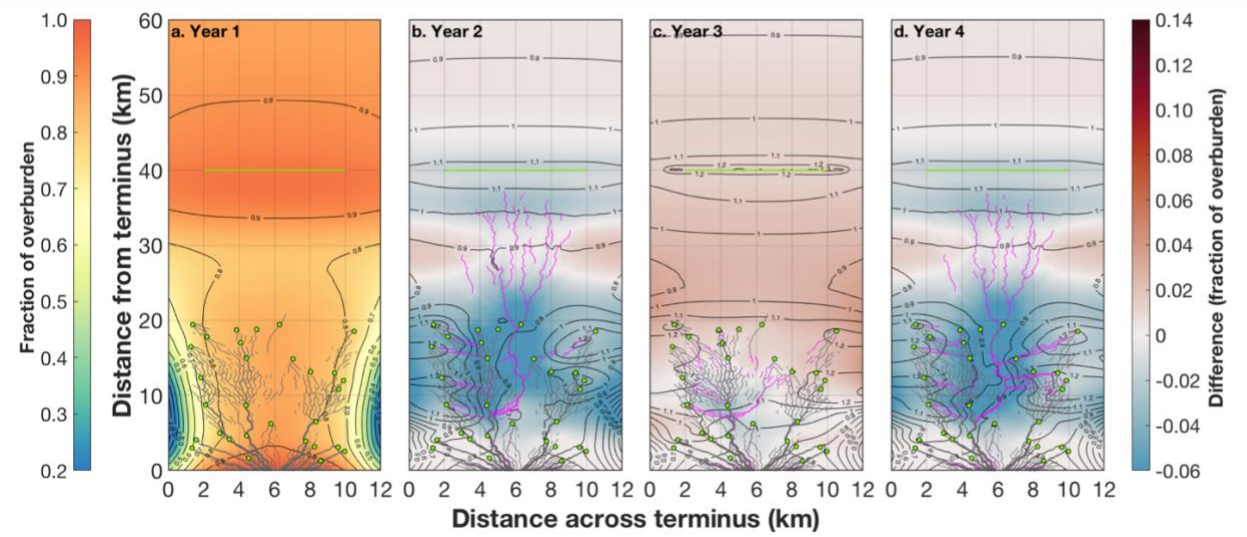

Figure S6. Evolution of subglacial water pressure for the firn aquifer seasonal ramp run, by year. (a–d) Same as Figure S2, except for the firn aquifer seasonal ramp input.

Figure S7. Spatial mean water pressure, composited by elevation.

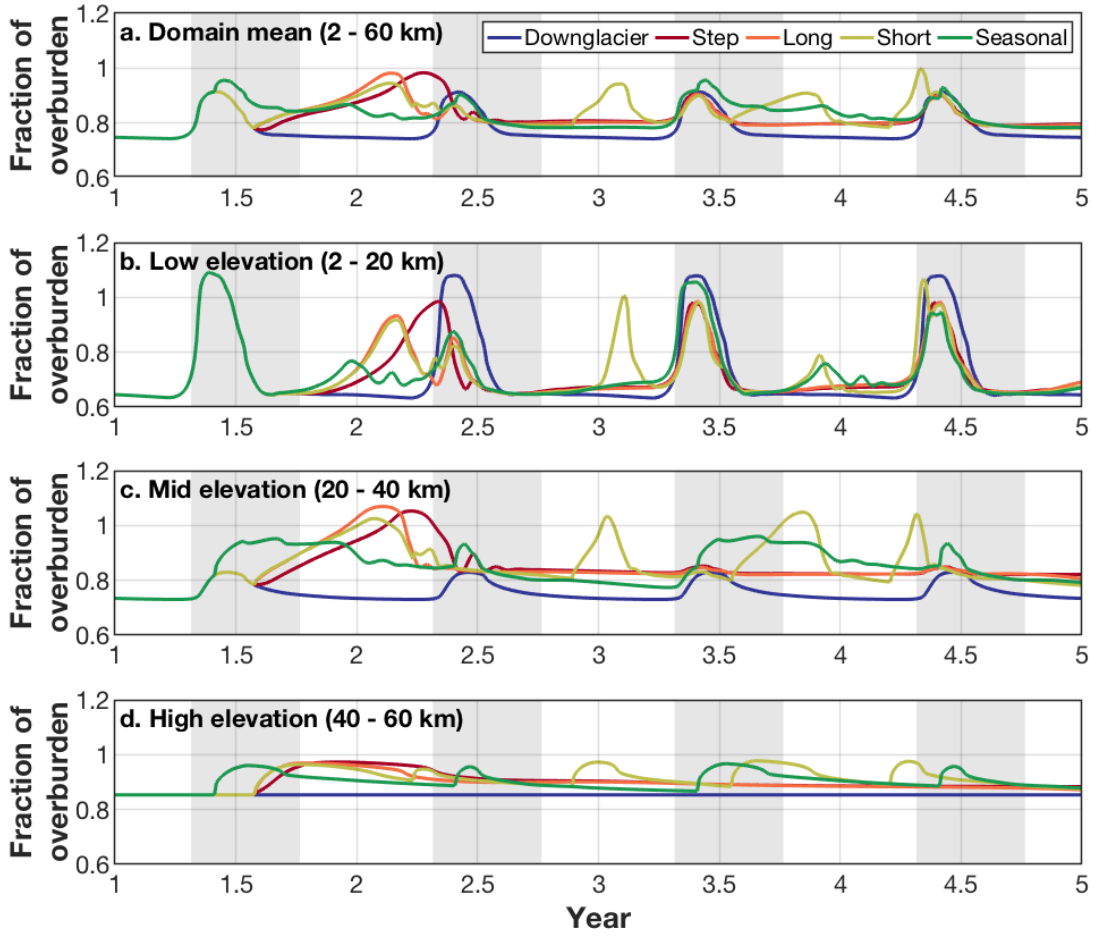

Figure S7. Average subglacial water pressure over time, composited by distances from the terminus. (a) Domain mean (2–60 km) fraction of overburden (b) Fraction of overburden averaged over the section of the model domain nearest the terminus (2–20 km), or low surface elevations (s < 900 m). (c) Fraction of overburden averaged over the middle of the model domain (20–40 km from the terminus), or moderate surface elevations (900 < s < 1500 m). (d) Fraction of overburden averaged over the uppermost section of the model domain (40–60 km from the terminus), or high surface elevations (1500 < s < 1800 m). In all panels, gray bars denote the melt season.

Figure S8. Residence time versus total channel area

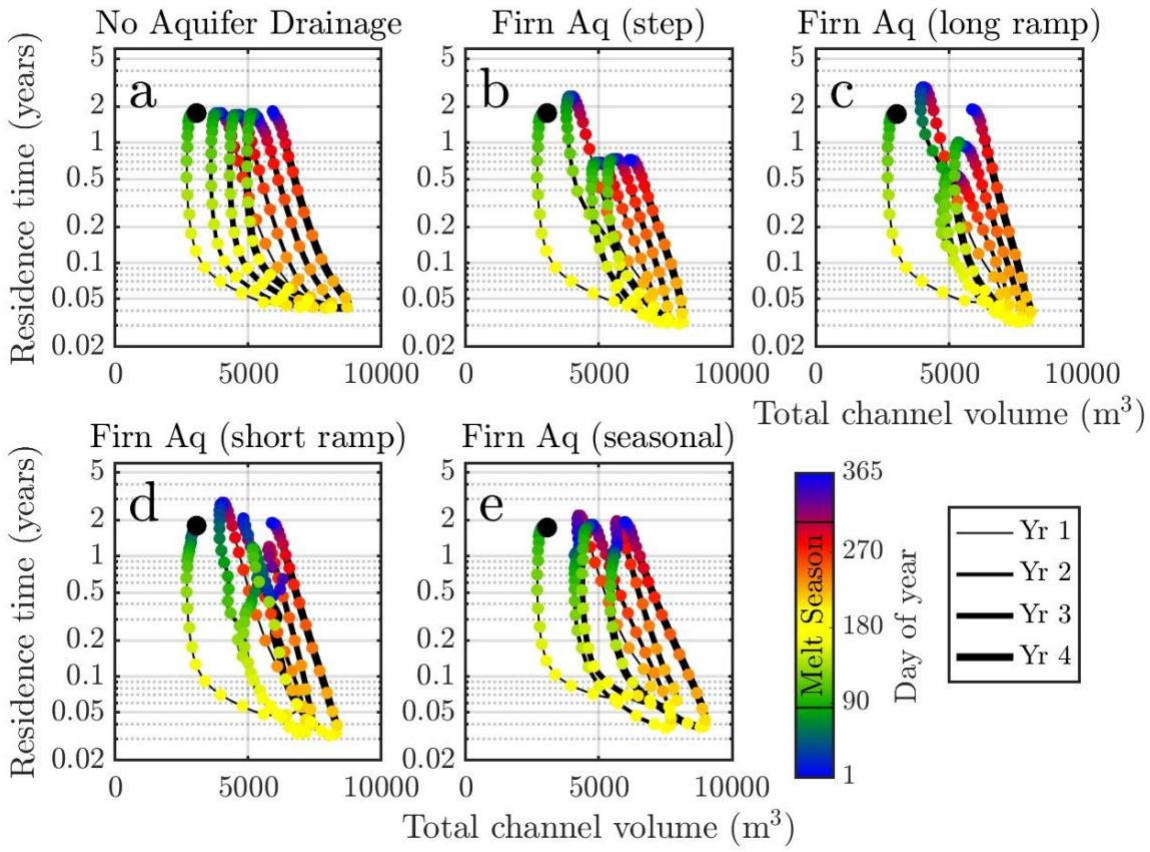

Figure S8. Phase diagrams showing the co-evolution of subglacial residence time and the total channel cross-sectional area summed across the model domain. Black dots show January 1 of Year 1 and time proceeds generally counter-clockwise. The black line thickness increases with each year. (a) Low-elevation inputs only; (b) Firn aquifer (step) run; (c) Firn aquifer (long ramp) run; (d) Firn aquifer (short ramp) run; and (e) Firn aquifer (seasonal ramp) run. In all model runs, the residence time decreased greatly over spring (green) and early summer (light green). Total channel size did not increase appreciably until mid to late summer (yellow), by when the channel size caused only a small further decrease in subglacial residence time. Addition of firn-aquifer water did not appreciably change the total channel size or the time of year (midsummer) at which it peaked, compared to the low-elevation run. In the firn-aquifer step function run (b), residence time remains low year-round (<1 year) after the second summer. In other runs with wintertime firn-aquifer water inputs (c and d), the wintertime residence times also remained shorter than in the low-elevation run.

Figure S9. Residence times of subglacial water, by season

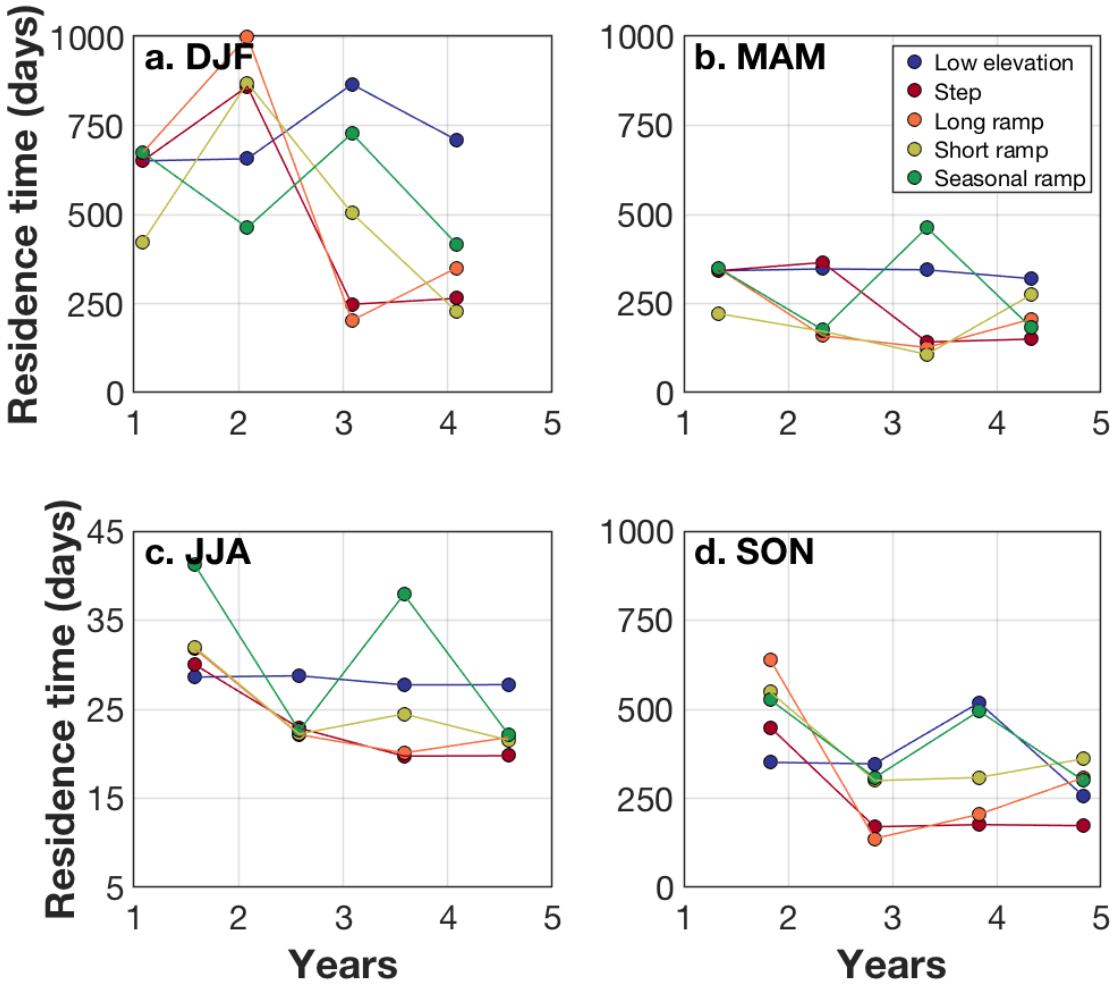

Figure S9. Seasonal residence times of subglacial meltwater. (a) Winter: December, January, February. (b) Spring: March, April, May. (c) Summer: June, July, August; this panel is shown in Figure 2g. (d) Autumn: September, October, November.

Figure S10. Sensitivity of subglacial system to geometry of glacier surface and bed

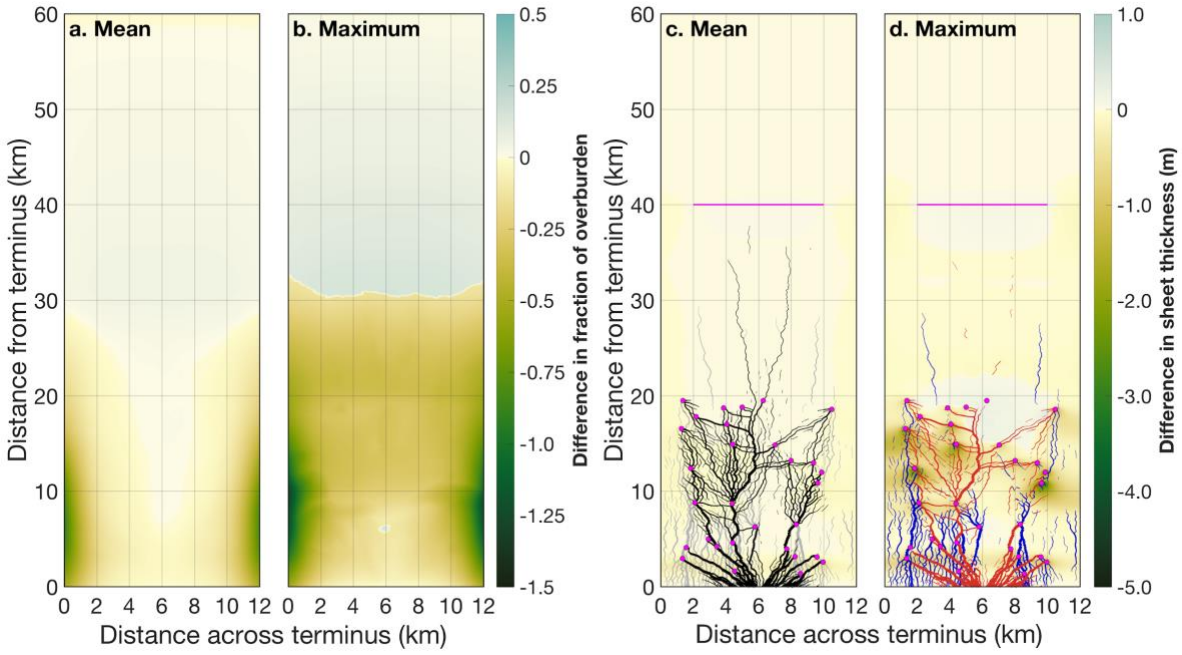

Figure S10. Sensitivity study comparing model runs with low-elevation water inputs across different model geometries (basal trough versus flat bed). (a) Mean difference in fraction of overburden pressure (basal trough run minus flat bed run). (b) Maximum difference. (c) Mean difference in sheet thickness (basal trough run minus flat bed run) with maximum channel extent (basal trough: black; flat bed: gray). (d) Maximum sheet thickness difference with difference in channel persistence. Colors on all panels indicate the difference between water pressure or sheet thickness for the basal trough and the flat bed geometries (basal trough run minus flat bed run). (d) Red lines indicate that channel persistence is greater in the basal trough run, with thicker lines indicating greater persistence. Blue lines indicate channel persistence is greater in the flat bed run, with thicker lines indicating greater persistence.

Figure S11. Sensitivity of subglacial system to ice velocity cap, using low-elevation inputs only

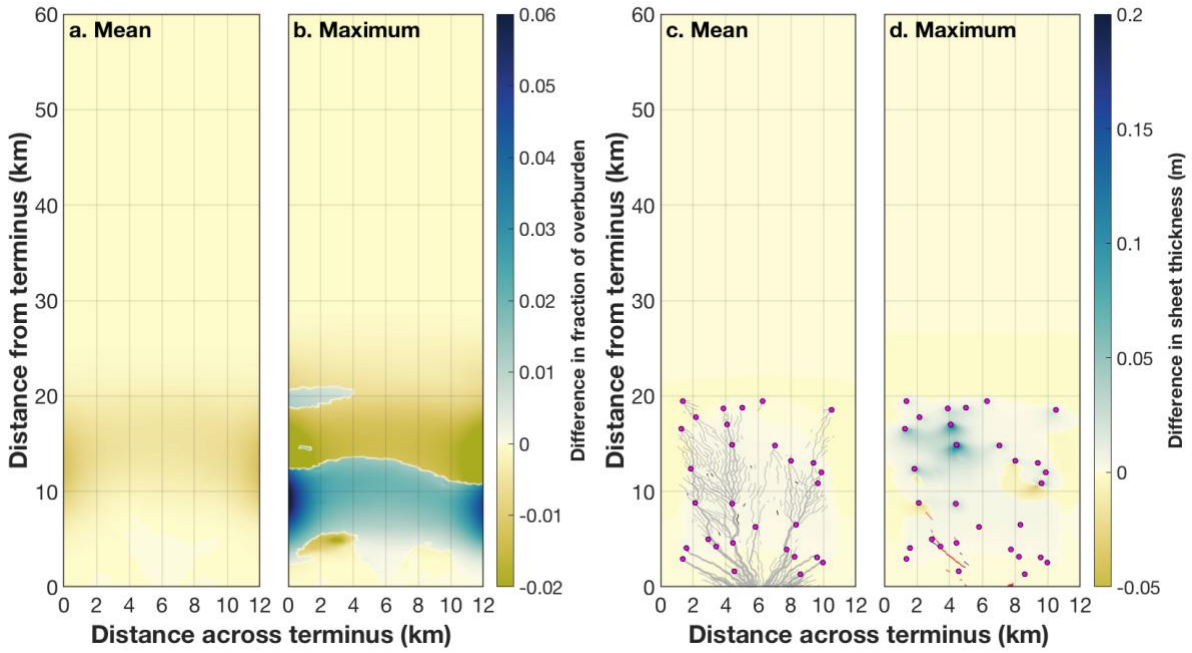

Figure S11. Same as Figure S10, but differences between 800 m·y^{-1} and 500 m·y^{-1} maximum ice speeds in model runs with low-elevation water inputs. (a) Mean difference in fraction of overburden pressure (800 m·y^{-1} run minus 500 m·y^{-1} run). (b) Maximum difference. (c) Mean difference in sheet thickness (800 m·y^{-1} run minus 500 m·y^{-1} run) with maximum channel extent (800m·y^{-1}: black; 500m·y^{-1}: gray). (d) Maximum sheet thickness difference with difference in channel persistence. Red lines indicate locations where channel persistence is greater in the 800m·y^{-1} run by 0.5–6%, with thicker lines indicating greater persistence. Blue lines indicate locations where channel persistence is greater in the 500m·y^{-1} run by 0.5–6%, with thicker lines indicating greater persistence.

Figure S12. Sensitivity of subglacial system to ice velocity cap, using firn-aquifer step inputs

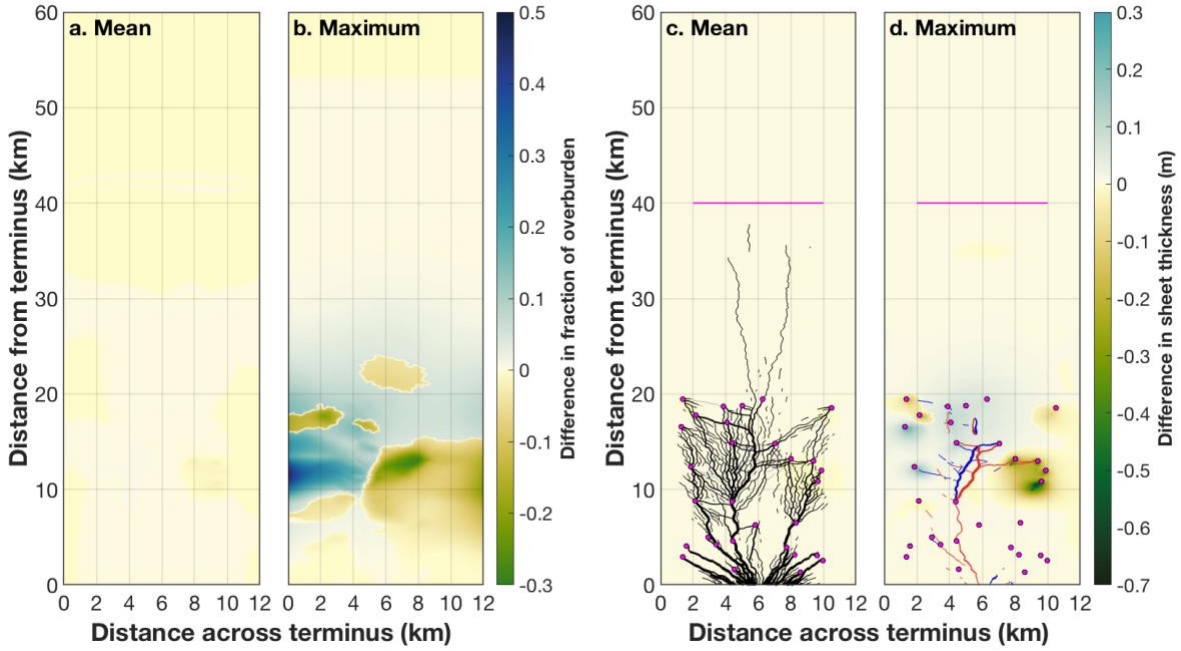

Figure S12. Same as Figure S11, except with step function firn-aquifer water inputs. (a) Mean difference in fraction of overburden pressure (800 $m \cdot y^{-1}$ run minus 500 $m \cdot y^{-1}$ run). (b) Maximum difference. (c) Mean difference in sheet thickness (800 $m \cdot y^{-1}$ run minus 500 $m \cdot y^{-1}$ run) with maximum channel extent (800$m \cdot y^{-1}$: black; 500$m \cdot y^{-1}$: gray). (d) Maximum sheet thickness difference with difference in channel persistence. Red lines indicate that channel persistence is greater in the 800$m \cdot y^{-1}$ run by 0.5–15%, with thicker lines indicating greater persistence. Blue lines indicate channel persistence is greater in the 500$m \cdot y^{-1}$ run by 0.5–15%, with thicker lines indicating greater persistence.

Figure S13. Ice flow speed boundary condition

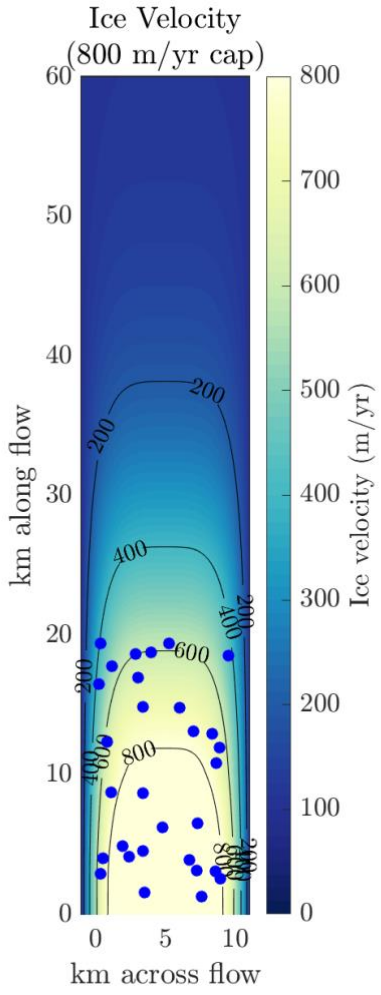

Figure S13. Plan view of ice speed applied across the model domain. Velocity is calculated using a quartic profile across flow and such that mass is conserved within our surface and bed geometries. Black contours show ice speed values in m/yr. Ice flow speed is capped at 800 m/yr.

Video S1.

Evolution of the subglacial water sheet thickness (top panels) over the four-year model run. Low-elevation water input locations are shown as blue dots in the lower 20 km of the domain; firn-aquifer input location as a red bar at 40 km. Top panels are low-elevation input, firn-aquifer step function, firn-aquifer seasonal ramp, firn-aquifer long ramp, and firn-aquifer short ramp, from left to right. Bottom panels show input hydrographs (upper) and the domain-averaged water sheet thickness time series (lower). Note the different scale for the low-elevation input hydrograph and the firn-aquifer input hydrographs.

Video S2.

Evolution of the subglacial water pressure field (top panels) over the four-year model run. Low-elevation water input locations are shown as blue dots in the lower 20 km of the domain; firn-aquifer input location as a red bar at 40 km. Top panels are low-elevation input, firn-aquifer step function, firn-aquifer seasonal ramp, firn-aquifer long ramp, and firn-aquifer short ramp, from left to right. Bottom panels show input hydrographs (upper) and the domain-averaged water pressure time series (lower). Note the different scale for the low-elevation input hydrograph and the firn-aquifer input hydrographs.

References

Aschwanden, A., Bueler, E., Khroulev, C. & Blatter, H. (2012), An enthalpy formulation for glaciers and ice sheets, *Journal of Glaciology*, *58*(209), 441–457, doi:10.3189/2012JoG11J088

Banwell, A. F., Willis, I. C. & Arnold, N. S. (2013), Modeling subglacial water routing at Paakitsoq, W Greenland, *Journal of Geophysical Research: Earth Surface*, 118(3), 1282–1295, doi:10.1002/jgrf.20093

Das, S. B., Joughin, I., Behn, M. D., Howat, I. M., King, M. A., Lizarralde, D., & Bhatia, M. P. (2008). Fracture Propagation to the Base of the Greenland Ice Sheet During Supraglacial Lake Drainage. *Science*, *320*(5877), 778–781. doi:10.1126/science.1153360

de Fleurian, B. et al. (2018), SHMIP: The Subglacial Hydrology Model Intercomparison Project, *Journal of Glaciology*, 467, 1–20, doi:10.1017/jog.2018.78

Dow, C. F. et al. (2015). Modeling of subglacial hydrological development following rapid supraglacial lake drainage. *Journal of Geophysical Research: Earth Surface*, *120*(6), 1127–1147. doi:10.1002/2014jf003333

Dow, C. F., Werder, M. A., Nowicki, S. & Walker, R. T. (2016), Modeling Antarctic subglacial lake filling and drainage cycles, *The Cryosphere*, 10, 1381–1393, doi:10.5194/tc-10-1381-2016

Dow C. F., Karlsson, N. B., & Werder, M. A. (2018). Limited impact of subglacial supercooling freeze-on for Greenland Ice Sheet stratigraphy. *Geophysical Research Letters*, 45. doi:10.1002/2017GL076251

Doyle, S. H., Hubbard, A. L., Dow, C. F., Jones, G. A., Fitzpatrick, A., Gusmeroli, A., et al. (2013). Ice tectonic deformation during the rapid in situ drainage of a supraglacial lake on the Greenland Ice Sheet. *The Cryosphere*, *7*(1), 129–140. doi:10.5194/tc-7-129-2013

Everett, A., Murray, T., Selmes, N., Rutt, I. C., Luckman, A., James, T. D., et al. (2016). Annual down-glacier drainage of lakes and water-filled crevasses at Helheim Glacier, southeast Greenland. *Journal of Geophysical Research: Earth Surface*, 1–15. doi:10.1002/2016JF003831

Gelaro, R., McCarty, W., Suarez, M. J., Todling, R., Molod, A., Takacs, L., et al. (2017). The Modern-Era Retrospective Analysis for Research and Applications, Version 2 (MERRA-2). *Journal of Climate*, *30*(14), 5419–5454. doi:10.1175/jcli-d-16-0758.1

Hoffman, M. J., Catania, G. A., Neumann, T. A., Andrews, L. C., & Rumrill, J. A. (2011). Links between acceleration, melting, and supraglacial lake drainage of the western Greenland Ice Sheet. *Journal of Geophysical Research: Solid Earth*, 116(F4). doi:10.1029/2010JF001934

Howat, I., Negrete, A. & Smith, B. E. (2014). The Greenland Ice Mapping Project (GIMP) land classification and surface elevation data sets. *The Cryosphere*, 8(4), 1509–1518. doi:10.5194/tc-8-1509-2014

Howat, I., Negrete, A. & Smith, B. (2015). *MEaSUREs Greenland Ice Mapping Project (GIMP) Digital Elevation Model, Version 1*. Boulder, Colorado USA. NASA National Snow and Ice Data Center Distributed Active Archive Center. doi:10.5067/NV34YUIXLP9W

Kehrl, L., I. Joughin, D. E. Shean, D. Floricioiu, & L. Krieger (2017). Seasonal and interannual variability in terminus position, glacier velocity, and surface elevation at Helheim and Kangerlussuaq Glaciers from 2008 to 2016. Journal of Geophysical Research, 122(9), 1635-1652. doi:10.1002/2016JF004133

MacGregor, J. A., Fahnestock, M. A., Catania, G. A., Aschwanden, A., Clow, G. D., Colgan, W. T., et al. (2016). A synthesis of the basal thermal state of the Greenland Ice Sheet. *Journal of Geophysical Research: Earth Surface*, 1–44. doi:10.1002/2015JF003803

McGrath, D., Colgan, W., Steffen, K., Lauffenburger, P., & Balog, J. (2011). Assessing the summer water budget of a moulin basin in the Sermeq Avannarleq ablation region, Greenland ice sheet. *Journal of Glaciology*, *57*(205), 954–964

Meierbachtol, T., Harper, J. & Humphrey, N. (2013). Basal Drainage System Response to Increasing Surface Melt on the Greenland Ice Sheet, *Science*, *341*(6147), 777–779, doi:10.1126/science.1235905

Moon, T., Joughin, I., Smith, B., Broeke, M. R., Berg, W. J., Noël, B., & Usher, M. (2014). Distinct patterns of seasonal Greenland glacier velocity. Geophysical Research Letters, 41(20), 7209–7216. doi:10.1002/2014GL061836.

Morlighem, M., E. Rignot, J. Mouginot, H. Seroussi, and E. Larour (2014). Deeply incised submarine glacial valleys beneath the Greenland ice sheet, *Nature Geoscience*, 7(6), 418–422, doi:10.1038/ngeo2167

Morlighem, M., Williams, C., Rignot, E., An, L., Arndt, J. E., Bamber, J., et al. (2017a). BedMachine v3: Complete bed topography and ocean bathymetry mapping of Greenland from multi-beam echo sounding combined with mass conservation, *Geophysical Research Letters*, 44, doi:10.1002/2017GL074954

Morlighem, M. et al. (2017b). *IceBridge BedMachine Greenland, Version 3*. Boulder, Colorado USA. NASA National Snow and Ice Data Center Distributed Active Archive Center. doi:10.5067/2CIX82HUV88Y

Phillips, T., Leyk, S., Rajaram, H., Colgan, W., Abdalati, W., McGrath, D. & Steffen, K. (2011), Modeling moulin distribution on Sermeq Avannarleq glacier using ASTER and WorldView imagery and fuzzy set theory, *Remote Sensing of the Environment*, 115(9), 2292–2301, doi:10.1016/j.rse.2011.04.029

Poinar, K., Joughin, I., Lilien, D., Brucker, L., Kehrl, L., & Nowicki, S. (2017). Drainage of Southeast Greenland Firn Aquifer Water through Crevasses to the Bed. *Frontiers in Earth Science*, *5*, 8–15. doi:10.3389/feart.2017.00005

Schoof, C. (2010). Ice-sheet acceleration driven by melt supply variability. *Nature*, *468*(7325), 803–806. doi:10.1038/nature09618

Smith, L. C., Chu, V. W., Yang, K., Gleason, C. J., Pitcher, L. H., Rennermalm, A. K., et al. (2015). Efficient meltwater drainage through supraglacial streams and rivers on the southwest Greenland ice sheet. *Proceedings of the National Academy of Sciences of the United States of America*, 201413024. doi:10.1073/pnas.1413024112

Werder, M. A., I. J. Hewitt, C. G. Schoof, and G. E. Flowers (2013), Modeling channelized and distributed subglacial drainage in two dimensions, *Journal of Geophysical Research: Earth Surface*, 118(4), 2140–2158, doi:10.1002/jgrf.20146

Wei, W., Greenbaum, J. S., Gourmelen, N., Dow, C. F., Bo, S., Guo, J., van Ommen, T. D., Roberts, J. L., Young, D. A., and Blankenship, D. D. (2018). The bathymetric and subglacial hydrological context for basal melting of the West Ice Shelf in East Antarctica. AGU Fall Meeting, 11 December 2018, San Francisco, C21C-1355